nature cell biology

Wdr1-mediated cell shape dynamics and cortical tension are essential for epidermal planar cell polarity

Chen Luxenburg[1,2,3], Evan Heller[1,3], H. Amalia Pasolli[1], Sophia Chai[1], Maria Nikolova[1], Nicole Stokes[1] and Elaine Fuchs[1,4]

During mouse development, core planar cell polarity (PCP) proteins become polarized in the epidermal plane to guide angling/morphogenesis of hair follicles. How PCP is established is poorly understood. Here, we identify a key role for Wdr1 (also known as Aip1), an F-actin-binding protein that enhances cofilin/destrin-mediated F-actin disassembly. We show that cofilin and destrin function redundantly in developing epidermis, but their combined depletion perturbs cell adhesion, cytokinesis, apicobasal polarity and PCP. Although *Wdr1* depletion accentuates single-loss-of-cofilin/destrin phenotypes, alone it resembles core PCP mutations. Seeking a mechanism, we find that Wdr1 and cofilin/destrin-mediated actomyosin remodelling are essential for generating or maintaining cortical tension within the developing epidermal sheet and driving the cell shape and planar orientation changes that accompany establishment of PCP in mammalian epidermis. Our findings suggest intriguing evolutionary parallels but mechanistic modifications to the distal wing hinge-mediated mechanical forces that drive cell shape change and orient PCP in the *Drosophila* wing disc.

PCP, the collective polarization of cells within a tissue plane, is an evolutionarily conserved hallmark of epithelial tissues[1–3]. Mouse skin development affords an excellent model to study the molecular mechanisms underlying this process in mammals. Epidermal cells use PCP as early as embryonic day 14.5 (E14.5), when core PCP proteins become asymmetrically localized along the anterior–posterior faces of basal layer cells[4]. When conserved PCP components *Fzd6* (*frizzled-6*), *Celsr1* (*flamingo*) and *Vangl2* (*strabismus*) are mutated, perturbations arise in anterior–posterior distributions of other PCP components leading to misangling of emerging hair follicles[4,5].

How PCP is established is still unfolding. In *Drosophila*, contraction of the developing wing hinge exposes wing-blade epithelial cells to anisotropic tension along the proximal–distal axis, which in turn, leads to oriented elongation, rearrangement and divisions that realign cell polarization along this axis[6]. Moreover, hinge severing eliminates these forces and alters tissue dynamics and PCP alignment. Whether mechanical forces function in PCP-driven events in other organisms/tissues and if so, by what molecular mechanisms, are unexplored questions in developmental biology[7].

Although not investigated in the context of mammalian PCP, pronounced changes in shape accompany the ability of mouse epidermal cells to maintain spindle orientation. Indeed, if progenitors within the innermost, basal layer cannot round up as they enter mitosis, spindle orientation defects arise[8]. *In vivo*, epidermal mitotic rounding is regulated by the actin-regulated transcription factor SRF (ref. 8). *In vitro*, Wdr1 is also involved[8–10]. Studies from other systems suggest that the effects of Wdr1 depend on its physical interaction with F-actin, as well as its association with members of the cofilin family of actin-binding proteins[11–17]. However, the mechanisms by which Wdr1 exerts its physiological roles in mammalian systems *in vivo* are poorly understood. In the mouse, its loss is lethal[18], whereas in yeast, it has no obvious phenotype[17].

In the present study, we show that, unexpectedly, *Wdr1* depletion in embryonic mouse epidermis results in a striking PCP phenotype. In pursuing a mechanism, we discovered that, like the *Drosophila* wing disc, mouse epidermal basal cells change their shape and orientation during PCP establishment. Combining laser ablation with video microscopy, we further show that coincident with the timing of

[1]The Rockefeller University, Howard Hughes Medical Institute, Laboratory of Mammalian Cell Biology and Development, New York, New York 10065, USA.
[2]Present address: Department of Cell and Developmental Biology, Sackler Faculty of Medicine, Tel Aviv University, Tel Aviv 69978, Israel. [3]These authors contributed equally to this work.
[4]Correspondence should be addressed to E.F. (e-mail: fuchslb@rockefeller.edu)

Received 1 September 2014; accepted 2 March 2015; published online 27 April 2015; DOI: 10.1038/ncb3146

PCP, cells within the developing epidermis are under tension. Finally, we show that Wdr1 is an important mediator of epidermal tension through its ability to promote cofilin-mediated actin severing, without which PCP cannot be established. Overall, our findings unravel important insights into the physiological roles of Wdr1-mediated actin dynamics and mechanical/geometrical cues in PCP.

RESULTS

Cytoskeletal and PCP phenotypes in Wdr1-deficient skin

To study the role of Wdr1 *in vivo*, we injected the amniotic sacs of E9.5 embryos *in utero* with high-titre lentivirus harbouring *Wdr1* or scramble short hairpin RNAs (shRNAs) and an H2B–GFP reporter gene[19] (Fig. 1a). Western blot and phalloidin (F-actin) staining of *Wdr1*-depleted basal cells revealed a striking increase in F-actin but not overall actin levels, consistent with the notion that Wdr1 functions as an enhancer of cofilin's F-actin severing activity (Fig. 1a–c). In control tissue, much of the F-actin was cortical and co-localized with E-cadherin. Without Wdr1, the belt of intense F-actin staining extended internally from the cell borders. Adhesion between neighbouring epidermal cells and adherence to their underlying basement membrane seemed to be normal, as judged by ultrastructural analysis (Supplementary Fig. 1). Wdr1-deficient epidermis also exhibited normal patterns of immunolabelling for adhesion proteins (β6 integrin, E-cadherin, ZO1), basement membrane protein (laminin-5) and apicobasal polarity markers (Par3 and centrosomes; Fig. 1c and Supplementary Fig. 2).

Probing deeper into the consequences of Wdr1 deficiency, we turned to the hair follicle. Instead of the characteristic anterior–posterior angling of their control counterparts, many of the follicles in *Wdr1*-368-transduced embryos grew straight downward (Fig. 1d). Quantifications revealed that in control backskins, <4% of hair follicles grew straight downward, whereas most hair follicles were oriented along the anterior–posterior axis (Fig. 1e,f). In contrast, nearly 30% of hair follicles pointed straight downwards in Wdr1-depleted epidermis, and for those that were angled, their orientation was broader than normal. Also lost were the anterior–posterior asymmetries of E-cadherin and P-cadherin expression at the follicle tip, and of NCAM along the posterior side of the follicle shaft (Fig. 1g).

Whole-mount immunofluorescence microscopy also revealed a loss of the typical elongation of anterior hair follicle cells relative to their posterior counterparts (Fig. 1h). These hair follicle defects are hallmarks of *looptail* and *crash* embryos[4], which harbour mutations in the core PCP genes, *Vangl2* and *Celsr1* (refs 20,21). Together, these data show that *Wdr1* depletion in skin results in most if not all typical PCP abnormalities, including loss of molecular and cell shape asymmetry of the basal epidermal cells at the juncture of hair follicle downgrowths, as well as randomization of follicle orientation within the developing hair coat.

Wdr1-depleted epidermis fails to establish PCP

To determine whether Wdr1 activity affects the localization of core PCP components, we analysed the distribution of Celsr1 between E13.5 and E15.5. Before PCP establishment (E13.5), this atypical cadherin was largely unpolarized in both control and Wdr1-deficient epidermis. By E14.5, however, Celsr1 polarization in control basal cells had jumped from <10 to 60%, and the typical angle of polarity was largely along the anterior–posterior axis (Fig. 2a–c). In contrast, Celsr1 distribution in the basal layer cells of Wdr1-deficient epidermis was noticeably perturbed. In some cells, its membrane localization was diminished (asterisk) whereas in others it was concentrated along the dorso-ventral axis (arrowhead). Quantifications showed that <30% of cells showed Celsr1 polarization, and those that did exhibited a broader angle of polarity than control cells (Fig. 2b,c). These defects were not attributable to a developmental delay in PCP, as perturbations were still evident at E15.5 (Fig. 2a). Moreover, the overall ratio between membrane and cytoplasmic intensities of both Celsr1 and E-cadherin was not altered (Fig. 2f), suggesting that these proteins maintain their cortical localization.

The PCP defects seen with *Wdr1-368* were recapitulated in embryos transduced with a second *Wdr1* shRNA (*Wdr1-1622*; Supplementary Fig. 3). Furthermore, a hairpin-resistant complementary DNA encoding a Wdr1–GFP protein rescued the *Wdr1*-knockdown (KD) PCP defects (Fig. 2c–e and Supplementary Fig. 4). These results validated the specificity of our findings, and underscored the importance of Wdr1 in the process.

Given the known link between cofilin family activity, adhesion and apicobasal polarity[13,22], we examined E-cadherin and Par3 immunolocalization (Fig. 2g). Importantly, the apical polarization of Par3 was maintained in *Wdr1*-KD epidermis, indicating that loss of Wdr1 does not result in a general loss of tissue polarity. Furthermore, by quantitative PCR (qPCR), levels of messenger RNAs encoding E-cadherin, PCP proteins and key apicobasal polarity and cytoskeletal genes were normal (Fig. 2h). Together, these results suggest that without Wdr1, the epidermis cannot establish PCP, even though it still expresses its core constituents and maintains apicobasal polarity.

Wdr1 cooperates with destrin/cofilin to establish planar and apicobasal polarity

Previous *in vitro* studies have demonstrated that Wdr1 is a potent enhancer of cofilin-mediated actin severing[10,23,24]. We thus explored the function of cofilin/destrin in establishing epidermal PCP and their relationship to Wdr1. In control epidermis, cofilin, destrin and Wdr1–GFP were all enriched at the periphery of basal cells (Fig. 3a). Their immunofluorescence patterns were not obviously perturbed in *Wdr1*-KD epidermis, suggesting that their general localization does not depend on Wdr1 in the skin (Supplementary Fig. 5a).

We next addressed whether epidermal loss of *Cfl1* and/or *Dstn* mimics the *Wdr1*-KD phenotype. To do so, we transduced E9.5 embryos *in utero* with shRNAs targeting *Cfl1* (Fig. 3b), and compared them with embryos harbouring a *Dstn* null allele ($Dstn^{corn1}$; refs 25,26). We examined E-cadherin and Par3 immunolocalization as indicators of apical polarization and adhesion. In E15.5 backskins lacking one of the two cofilins, E-cadherin localization remained membranous, and the apical polarization of Par3 was maintained (Fig. 3c,d). In these single mutants, the number of cells exhibiting Celsr1 anterior–posterior enrichment decreased subtly from 63% in control E15.5 epidermis to 52% and 55% respectively (Fig. 3c,d,g). However, a long-range Celsr1 labelling pattern was established in these mutants.

To address the possibility that *Cfl1* and *Dstn* function redundantly in the skin, we knocked down *Cfl1* in $Dstn^{corn1}$ embryos. In sharp contrast to single depletions, removal of both proteins resulted in

defects in adhesion, apicobasal polarity, cytokinesis and PCP (Fig. 3e). Par3 localization within the basal layer was no longer excluded from the basal membrane. The typical PCP patterning of Celsr1 was also grossly disrupted, with more than a tenfold decrease in the number of polarized cells (Fig. 3e,g).

In contrast to double cofilin/destrin deficiency, Wdr1 deficiency affected planar polarity but not apicobasal polarity (Figs 2a–g and 3e). However, knockdown of *Wdr1* in *Dstn*^{corn1} mice (*Dstn*KO+*Wdr1*) yielded a phenotype similar to those of cofilin/destrin double mutants, where both apicobasal and planar polarity were grossly perturbed (Fig. 3f,g). The effects of destrin, cofilin and Wdr1 on PCP were quantified and are presented in Fig. 3g. These data underscore the impact of Wdr1 on cofilin/destrin function. They further suggest that when Wdr1 is absent, the F-actin-severing activity imparted by one of the cofilin/destrin pair is not sufficiently high to compensate for loss of the other.

If Wdr1 functions primarily to enhance cofilin/destrin activity, then overexpressing a constitutively active mutant of cofilin (CflS3A–GFP; ref. 27) might be expected to compensate for the loss of Wdr1. Although purified CflS3A does not exhibit enhanced enzymatic activity relative to wild-type cofilin[28], its overexpression in cells is expected to increase F-actin severing by increasing the pool of cofilin capable of binding and severing actin[29].

Indeed, CflS3A–GFP restored Celsr1 localization in *Wdr1*-KD embryos to the anterior–posterior pattern typical of PCP (Fig. 4a,c). This was particularly intriguing, given that in wild-type embryos, constitutively active cofilin caused subtle perturbations in both apicobasal and planar cell polarity (Fig. 4b,c). Supplementary Table 1 summarizes the phenotypic analyses of the data from Figs 3 and 4. Together, these data suggest that Wdr1 is a critical enhancer of cofilin activity, which in turn must be tightly balanced for proper PCP establishment.

Wdr1 is required for efficient F-actin severing in keratinocytes

How Wdr1 enhances cofilin activity is not fully understood. Several potential mechanisms have been proposed, including inhibiting the elongation of ADP–actin filaments with capping protein[23] and enhancing the lateral displacement of cofilin to promote actin severing[10]. It is nevertheless well established that Wdr1 has no catalytic activity of its own and that it exerts its role by interacting with both actin filaments and cofilins.

To dig deeper into the link between the cytoskeletal and PCP phenotypes of Wdr1-depleted epidermis and cofilin-mediated actin severing, we first examined endogenous levels of active (unphosphorylated) and inactive (phosphorylated) cofilin in lysates of cells expressing control and *Wdr1* shRNAs, as well as cells overexpressing CflS3A–GFP in both a control and Wdr1-depleted background. Wdr1-depleted cells exhibited a ∼1.3-fold increase in endogenous cofilin levels (Fig. 5a and Supplementary Figs 5c and 6a). This was surprising, because phalloidin staining in sagittal sections had indicated an increase in F-actin (Fig. 1c). Indeed, western blot analysis in Wdr1-depleted keratinocytes showed a ∼2-fold increase in F-actin content (Fig. 5b and Supplementary Fig. 6b). Moreover, F-actin levels were restored to near wild-type levels when CflS3A–GFP was overexpressed in *Wdr1*-KD cells. These results are consistent with previous *in vitro* studies suggesting that Wdr1 regulates actin severing not by modulating the pool of cofilin capable of binding actin through phosphorylation, but rather as a direct enhancer of cofilin-mediated actin severing[10,23,24]. Supporting this, the ability of Wdr1-depleted cell lysates to sever exogenous, pyrene-labelled F-actin was reduced in comparison with scramble-shRNA controls, and could be rescued by CflS3A–GFP overexpression (Fig. 5c).

Wdr1 does not affect trafficking of PCP proteins

In contemplating how Wdr1 might affect PCP, we were intrigued by a recent report that depletion of Cfl1 in *looptail* (*Vangl2*) mutant mice accentuates PCP defects within the node and midline cells of early post-gastrulation (E9.5) mouse embryos[30]. In that case, *Cfl1* depletion seemed to exacerbate the PCP phenotype by perturbing the planar-polarized trafficking of Rab11+ vesicles to the apical membrane.

In the epidermis, Rab11 is involved in the recycling of PCP proteins during mitosis[31]. In E14.5 *Wdr1*-depleted backskin, however, both Rab11 localization and Celsr1 mitotic internalization seemed to be unperturbed (Fig. 6a,b). This was also true under destrin/cofilin-deficient conditions (Fig. 6c). Furthermore, mitotic epidermal cells of Wdr1–GFP-transduced embryos revealed no obvious signs of Wdr1 internalization into Celsr1-containing vesicles (Fig. 6d).

We also pursued possible parallels to loss-of-function defects in *flare*, the *Drosophila* orthologue of *Wdr1*. *Flare* mutants exhibit a complex phenotype involving cell proliferation, viability and PCP defects[32]. Despite similarities in PCP defects, *Wdr1* KD differed from *Flare* in showing seemingly unperturbed cell proliferation, viability and differentiation in the developing mouse epidermis (Fig. 6e,f). Moreover, *Wdr1* KD did not overtly perturb the microtubule cytoskeleton, which has been reported to affect PCP in *Drosophila* by regulating the delivery of core PCP proteins[33]. *Wdr1* KD also showed no alterations in the primary cilium, some of whose components have been genetically linked to PCP defects[34] (Fig. 6g).

Overall, these results suggest that destrin/cofilin and/or Wdr1 may affect PCP differently in different organisms, tissues and/or developmental windows. Our findings suggest that Wdr1 and destrin/cofilin do not exhibit the typical behaviour of core PCP components (anterior–posterior localization/polarized recycling), but rather act as mediators of PCP. We therefore returned our focus to the loss of PCP-mediated asymmetries in *Wdr1*-depleted hair follicles (Fig. 1e) and the aberrations in mitotic rounding of basal epidermal cells (Fig. 1c and Supplementary Fig. 9). These defects in cell shape were of particular interest given that in the *Drosophila* wing disc, global cell shape dynamics are coupled to PCP reorientation[6].

Cell shape dynamics are regulated by *Wdr1* and coincide with PCP establishment

Although developmental cell shape changes have not been previously described within the plane of the mouse epidermal sheet, we wondered whether they might have been hitherto overlooked. To examine this, we used E-cadherin immunolabelling to delineate the epidermal cell borders of control and *Wdr1*-depleted embryos during the period when PCP is established. Surprisingly, automated analyses of cell shape revealed that from E12.5 (non-polarized epidermis) to E13.5 (partially polarized) to E14.5 (polarized)[4], normal basal cells indeed underwent a striking change in both their shape and orientation (Fig. 7a–d). During this process, cells decreased their surface area (from 59.9 ± 0.8

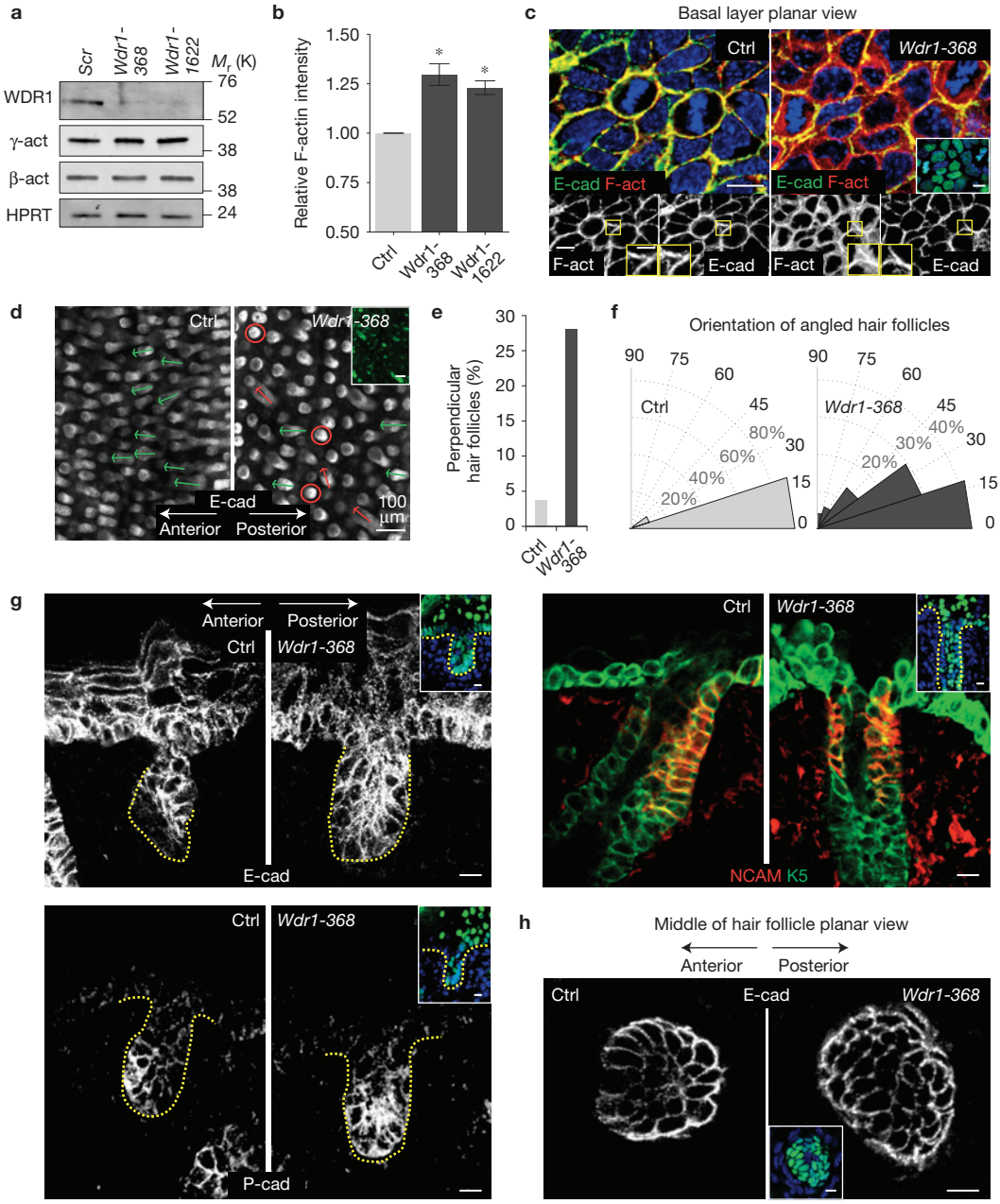

Figure 1 Depletion of Wdr1 alters the cytoskeleton and yields a PCP phenotype. (**a**) Immunoblot of primary mouse keratinocytes infected with *Scr*, *Wdr1-368* or *Wdr1-1622* shRNAs and probed with Wdr1, β-actin or γ-actin and HPRT (loading control) antibodies. (**b**) FACS analysis of F-actin (phalloidin) relative intensity in control versus *Wdr1-368* and control versus *Wdr1-1622*-depleted primary mouse keratinocytes. Error bars represent s.d. for $n=3$ independent experiments per sample. $P=0.032$, control versus *Wdr1-368*; $P=0.022$, control versus *Wdr1-1622* (independent, unpaired *t*-tests). Asterisks indicate statistical significance at $P<0.05$. (**c**) Whole-mount immunofluorescence of E15.5 embryos labelled for E-cadherin (E-cad), F-actin (F-act) and 2-(4-amidinophenyl)-6-indolecarbamidine dihydrochloride (DAPI, in blue) and imaged in the mid-plane of the basal layer. (**d**) Whole-mount anti-E-cadherin immunofluorescence of E18.5 backskin in control and Wdr1 KD imaged in a plane parallel to the skin surface but near the base of downgrowing hair follicles. Circles denote perpendicular orientations; arrows denote hair follicle angling (green, normal; red, perturbed). (**e**,**f**) Quantifications of data shown in **d**. Control, $n=325$; Wdr1, $n=412$ hair follicles from 3 embryos per condition. (**g**) Immunofluorescence of control and *Wdr1*-KD hair follicles stained for E-cadherin (E-cad) and P-cadherin (P-cad) and co-labelled for NCAM and keratin 5 (K5). (**h**) Whole-mount anti-E-cadherin immunofluorescence of control and *Wdr1*-KD hair follicles imaged through a plane at the bottom of the hair follicle. Yellow outlines and inset in **c** show digital magnification (×2) of F-actin/E-cadherin staining. Insets in **c**, **g** and **h** show that the region imaged was transduced (H2B–GFP+ nuclei). Scale bars, 10 μm (**c**,**g**,**h**) and 100 μm (**d**). Uncropped images of blots are shown in Supplementary Fig. 6.

to $51.7\pm0.8\,\mu m^{-2}$) and became less elongated (from 0.44 ± 0.006 to 0.37 ± 0.006). Moreover, cells underwent a reorientation from the dorso-ventral to anterior–posterior axis by E14.5.

In *Wdr1*-KD epidermis, these shape changes did not take place, and cells failed to reorient as in wild-type embryos (Fig. 7a,e–g). At E14.5, *Wdr1*-depleted cells were also less columnar than their

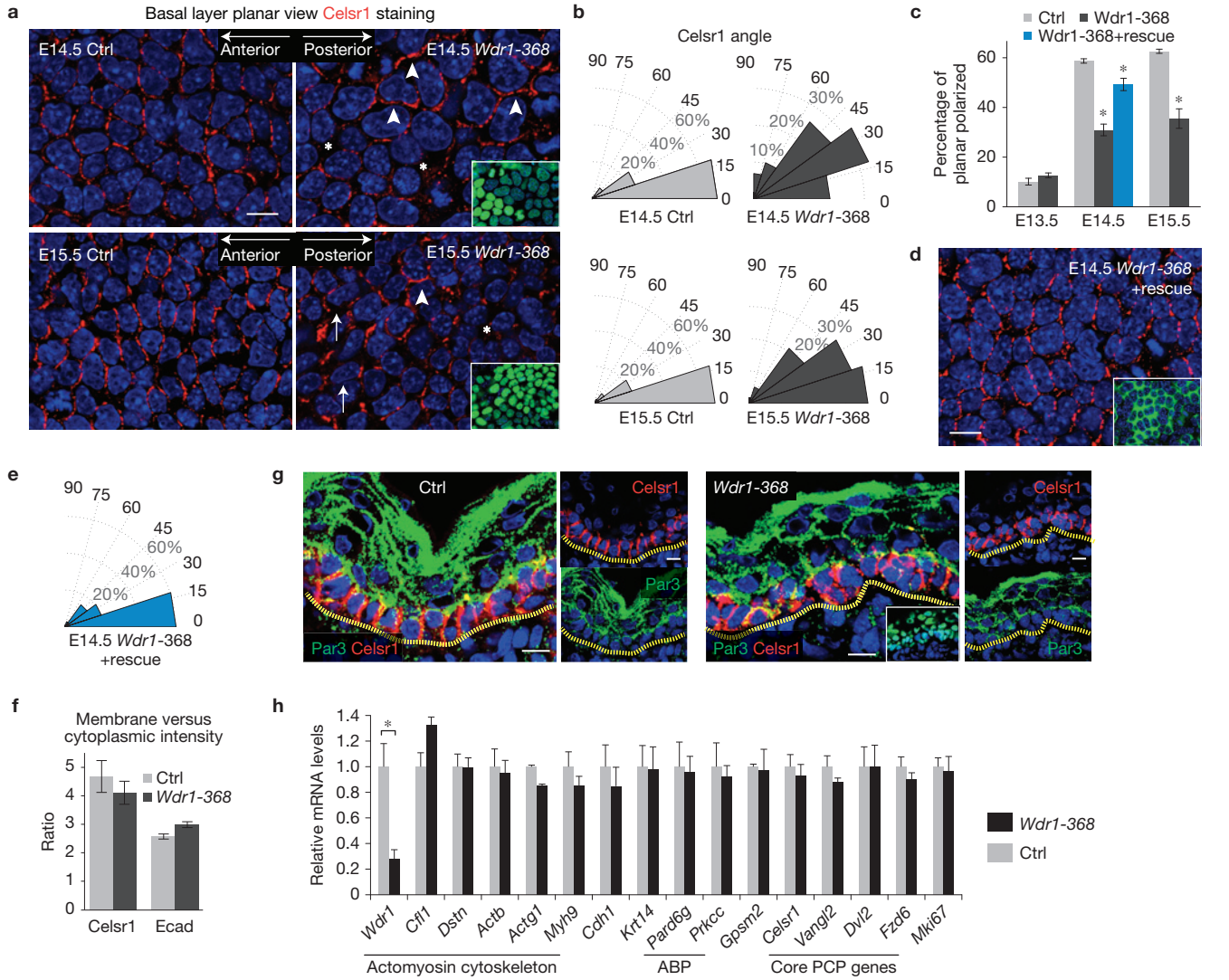

Figure 2 *Wdr1*-depleted epidermis fails to establish PCP. (**a**) Whole-mount immunofluorescence of E14.5 and E15.5 backskins from control and *Wdr1*-KD embryos labelled for Celsr1 and DAPI and imaged in the mid-plane of the basal layer. Arrowheads indicate normally planar polarization, arrows indicate misoriented polarity, asterisks indicate absence of polarity. (**b**) Histograms of the orientation of Celsr1 relative to the anterior–posterior axis. Measurements are pooled from 3 embryos. E14.5 control, $n=197$ cells; E14.5 Wdr1-368, $n=192$ cells; E15.5 control, $n=145$ cells; E15.5 Wdr1-368, $n=157$ cells. (**c**) Quantification of the percentage of planar-polarized cells from $n=3$ embryos per condition. $P=0.29$ (Wdr1 versus Ctrl, E13.5), 0.00012 (Wdr1 versus Ctrl, E14.5), 0.0103 (Wdr1+rescue versus Ctrl), 0.026 (Wdr1 versus Ctrl, E15.5), ANOVA followed by Tukey's HSD test. Asterisks indicate statistical significance at $P<0.05$. (**d**) Rescue data showing that the *Wdr1*-depletion phenotype can be compensated for by Wdr1–GFP. (**e**) Quantification of data from **d**, $n=201$ cells pooled from 3 embryos. (**f**) Quantifications of membrane versus cytoplasmic immunofluorescence intensities of Celsr1 and E-cadherin in E14.5 basal epidermis. There is no significant loss of Celsr1 at the membrane in *Wdr1*-KD epidermis ($P=0.4315$, unpaired *t*-test, $n=8$ frames of ~200 cells from 4 embryos for Wdr1 KD, $n=5$ frames from 2 embryos for Ctrl). (**g**) Sagittal views of 10 μm sections of Ctrl and *Wdr1*-KD E16.5 backskins immunolabelled for Celsr1 and Par3. Dotted lines denote dermal–epidermal border. (**h**) qPCR of mRNAs from FACS-purified, E14.5 basal epidermal progenitors from *Wdr1-368*- and *scramble*- (Ctrl) transduced E14.5 embryos, $n=3$ embryos per condition. A statistically significant change was detected only in Wdr1 mRNA levels (1 ± 0.18 versus 0.28 ± 0.07, $P=0.0002$, unpaired *t*-test). ABP, apicobasal polarity. Insets in **a**,**d** show that the region imaged was transduced (H2B–GFP+ nuclei). Error bars indicate mean ± s.e.m. Asterisks in **c** and **h** indicate statistical significance at $P<0.05$, scale bars, 10 μm.

wild-type counterparts (Fig. 7g). Notably, a hairpin-resistant cDNA encoding a Wdr1–GFP protein rescued the *Wdr1*-KD cell area defects (Fig. 7a,e), underscoring the specificity of Wdr1 in effecting these cell shape changes.

In the *Drosophila* wing disc, external mechanical forces from the distant wing hinge drive both tissue dynamics and PCP alignment[6]. In mammalian epidermis, there is no apparent analogy for the forces exerted by the wing hinge. However, Wdr1-depleted mouse epidermis did exhibit defects in F-actin content and organization (Fig. 1), which is known to affect myosin II activity[35] and therefore a cell's ability to generate tension. Moreover, Wdr1 is essential for the assembly of contractile actin networks in the *Caenorhabditis elegans* myoepithelial sheath[36], the ability of the mouse heart to contract[37], and to recruit myosin II to the contractile ring during cytokinesis[10]. This prompted

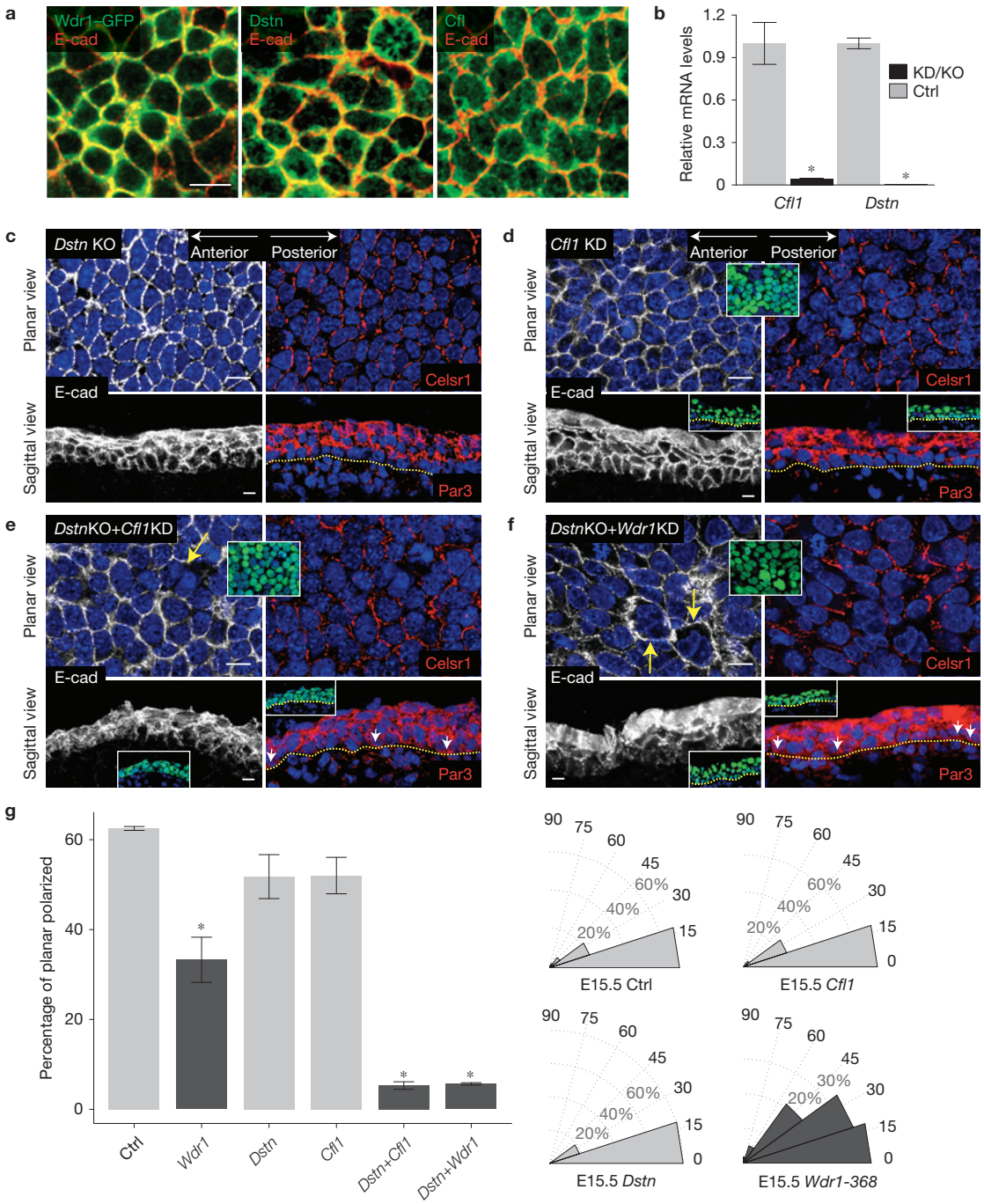

Figure 3 Molecular genetic analyses illuminate roles for the Wdr1-cofilin/destrin pathway in apicobasal and planar cell polarity. (**a**) Whole-mount immunofluorescence of basal layer cells in E15.5 backskin co-labelled for E-cadherin and WDR1–GFP or destrin (Dstn) or cofilin (Cfl1) and imaged within the mid-plane of the basal layer. (**b**) qPCR of mRNAs from control and *Cfl1*KD/*Dstn*-null (KD/KO) primary mouse keratinocytes, $n=3$ samples per condition. $P=0.0026$ (Cfl1 levels, Ctrl versus KD); $P=0.009$ (Dstn levels in Ctrl versus KO), unpaired *t*-test. (**c**–**f**) Whole-mount immunofluorescence of E15.5 backskins co-labelled for E-cadherin and Celsr1. Sagittal views are of 10 μm sections of E15.5 backskin immunolabelled for E-cadherin and Par3. Data are for the following genetic manipulations: *Dstn* KO (**c**), *Cfl1* KD (**d**), *Dstn*KO+*Cfl1*KD (**e**), *Dstn*KO+*Wdr1-368* (**f**). (**g**) Quantifications of the data shown in **c**–**f**. For the percentage of planar-polarized cells, $P=0.0014$ (*Wdr1* versus Ctrl), 0.6487 (*Dstn* versus Ctrl), 0.5766 (*Cfl1* versus Ctrl), 3×10^{-7} (*Cfl1*+*Dstn* versus Ctrl), 4×10^{-7} (*Wdr1*+*Dstn* versus Ctrl), ANOVA followed by Tukey's HSD test, $n=3$ embryos per condition. For histograms, $n=91$ cells (Ctrl); $n=135$ cells (*Cfl1*); $n=104$ cells (*Dstn*); $n=82$ cells (*Wdr1-368*). Yellow arrows denote bi/multinucleated cells, occasionally noted in the double mutants; white arrows denote abnormal Par3 localization along the basal surface of progenitor cells. Error bars indicate mean ± s.e.m. Asterisks indicate statistical significance at $P<0.05$. Scale bars, 10 μm.

us to wonder whether Wdr1 might also regulate tension within the mammalian epidermis.

To test this, we added a membrane GFP marker[38] to our lentiviral vectors, and repeated transductions as before.

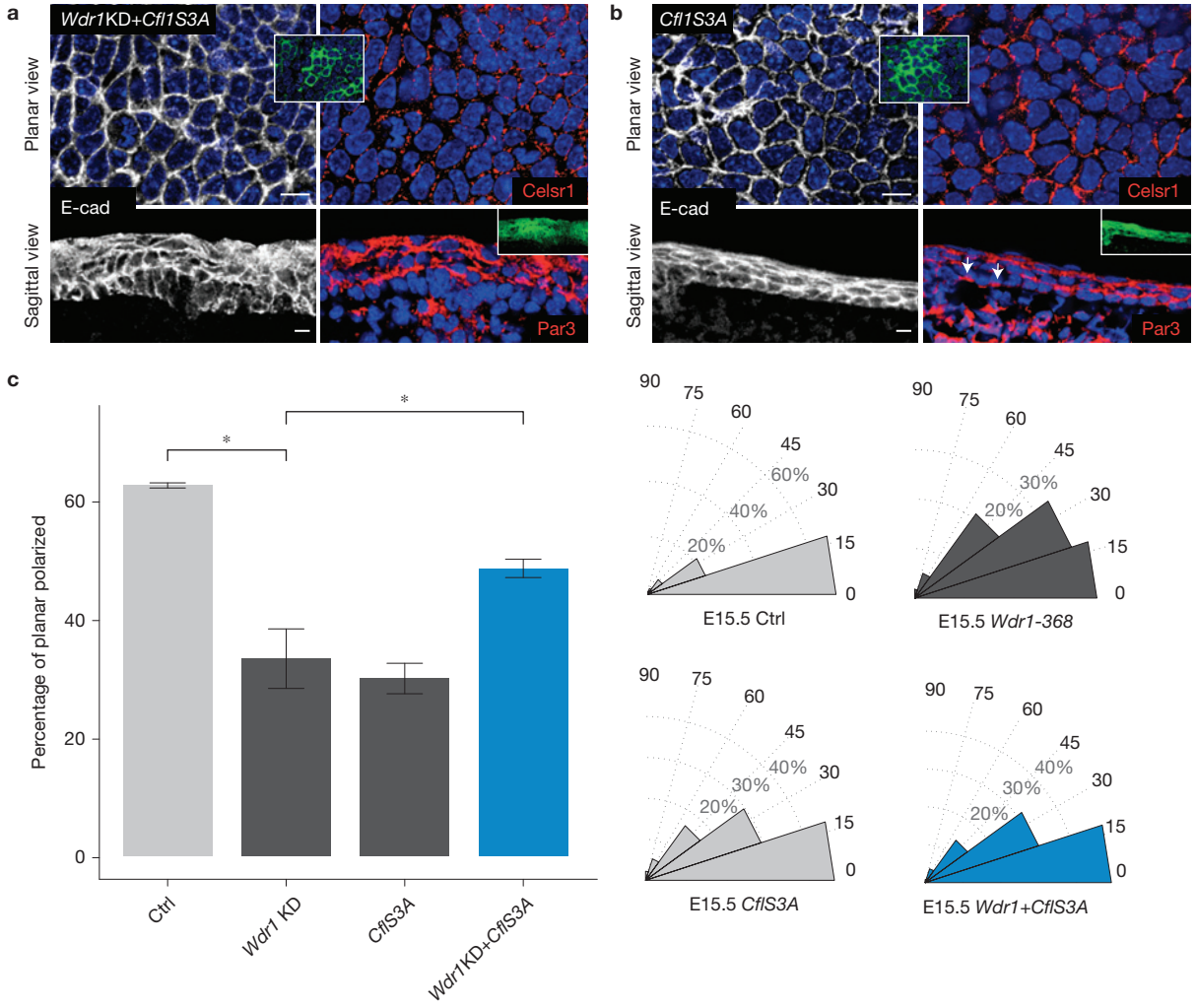

Figure 4 Rescue of the planar polarity defects of Wdr1 mutants by expression of constitutively active cofilin. (**a**,**b**) Whole-mount immunofluorescence of E15.5 backskins co-labelled for E-cadherin and Celsr1 or sagittal views labelled with E-cadherin and Par3. (**a**) *Wdr1-368*+*Cfl1S3A* overexpression. (**b**) *Cfl1S3A* overexpression. (**c**) Quantification of data shown in **a**,**b**. For the percentage of planar-polarized cells, $P = 0.00142$ (*Wdr1* versus Ctrl), 0.00207 (*Cfl1S3A* versus Ctrl), 0.247 (*Wdr1*+*Cfl1S3A* versus Ctrl), 0.0479 (*Wdr1* versus *Wdr1*+*CflS3A*), ANOVA followed by Tukey's HSD test, $n = 3$ embryos per condition. For histograms, $n = 91$ cells (Ctrl); $n = 82$ cells (*Wdr1-368*); $n = 131$ cells (*Cfl1S3A*); $n = 176$ cells (*Wdr1*KD+*Cfl1S3A*). Error bars indicate mean ± s.e.m. Asterisks indicate statistical significance at $P < 0.05$. Scale bars, 10 μm.

Wdr1 activity is essential for cell ability to generate/maintain cortical tension

At E14.5, embryos were subjected to laser ablation and imaging *ex vivo* to estimate tension in the epidermis (Fig. 8a). In *scramble*-shRNA control skin, laser ablation of membrane and cortical cytoskeleton[39–41] at a basal cell–cell interface yielded a mean initial retraction velocity (a quantity proportional to tension) of 0.214 μm s^{-1} versus 0.0534 μm s^{-1} in Wdr1-deficient epidermis (Fig. 8b). Similar results were obtained when cells were ablated along the anterior–posterior or dorsal–ventral axes.

To explore the link between Wdr1, actin severing, cortical tension and the establishment of PCP, we investigated whether CflS3A–GFP, which rescues actin severing in Wdr1-depleted keratinocytes, can also rescue the cortical tension defects of *Wdr1*-KD epidermis. In contrast to *Wdr1* KD alone, *Wdr1*KD+CflS3A–GFP epidermis showed an initial retraction velocity of laser-ablated cell junctions that was essentially equivalent to scramble-shRNA epidermis (0.266 μm s^{-1} versus 0.214 μm s^{-1}, Fig. 8b). These findings imply a relationship between the regulation of actin severing and tension by Wdr1 and its role in establishing PCP.

Consistent with this notion, loss of Wdr1 resulted in a striking reduction in the localization of myosin II at the cortex of basal epidermal cells (Fig. 8c). Compared with adjacent, untransduced regions (Fig. 8c, left), which exhibited tight localization of myosin II at the cortex, the myosin IIA network of *Wdr1*-KD cells was more diffuse and extended into the cell interior (Fig. 8c, right).

If the tension defects we see in Wdr1-depleted epidermis reflect perturbations in actomyosin-derived tension, then altering myosin II function[10] should generate similar defects. Although expression of multiple myosin II genes in embryonic epidermis precluded genetic analysis, we repeated our assays in E14.5 embryos exposed to either blebbistatin, which inhibits myosin II motor activity[42], or Y27632,

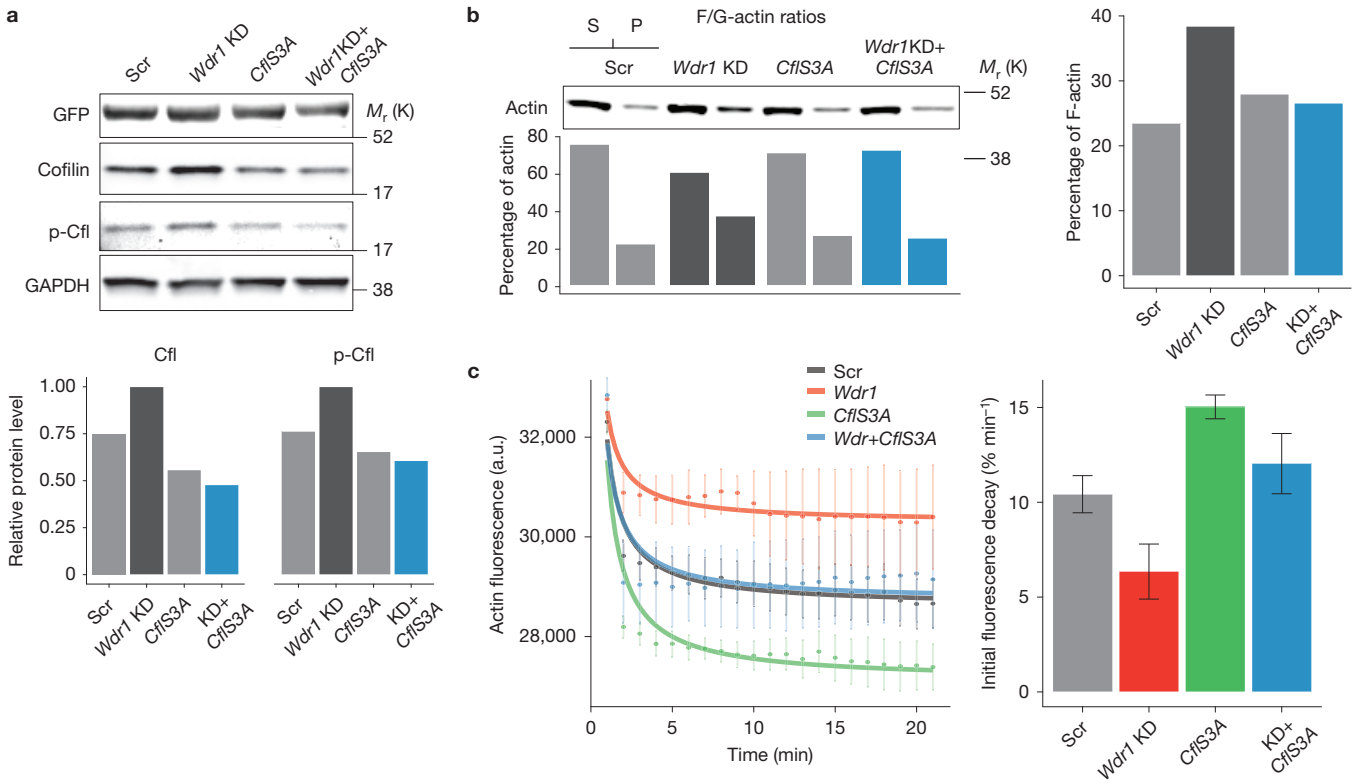

Figure 5 *Wdr1* is required for efficient F-actin severing in keratinocytes. (**a**) Western blots illustrating endogenous levels of active (unphosphorylated) and inactive (phosphorylated) cofilin in *Wdr1-368*-, CfIS3A–GFP- and *Wdr1*+CfIS3A–GFP-expressing keratinocytes. Note that histone H2B–GFP was contained within the same vectors as Scramble and *Wdr1-368* shRNAs, but not CfIS3A–GFP. Quantifications of bands, normalized for GAPDH, are provided below. (**b**) Loss of *Wdr1* is associated with an increase in F-actin, and normal F-actin levels are restored when CfIS3A–GFP is expressed in *Wdr1*-KD keratinocytes. F-actin (pellet), G-actin (supernatant) and total actin levels were determined by quantifying western blots and normalizing against control proteins (see Supplementary Fig. 6). (**c**) Pyrene F-actin severing assay illustrating that Wdr1 is required for efficient F-actin severing. The rate of fluorescence quenching can be restored in *Wdr1*-KD keratinocytes by overexpression of CfIS3A–GFP. Rates are determined by a linear fit to the initial part of the plot. Data represent the mean ± s.e.m. from $n=4$ independent measurements. Uncropped images of blots are shown in Supplementary Fig. 6.

which inhibits Rho kinase[43]. Indeed, these inhibitors resulted in modest increases in planar cell area and boundary tension defects similar to the loss of Wdr1 (Fig. 8d,e).

Given the increase in F-actin we observed in the absence of Wdr1, we repeated our assays in E14.5 embryos exposed to jasplakinolide, a drug that stabilizes F-actin and leads to its ectopic accumulation[44]. Both cell area and boundary tension defects were nearly identical to those of *Wdr1*-KD embryos (Fig. 8d,e), illustrating that increasing F-actin levels in the epidermis leads to a reduction in cortical tension. Importantly, each of these pharmacological perturbations resulted in a disruption in planar polarity compared with dimethylsulphoxide (DMSO)-treated embryos, with Celsr1 acquiring a more uniform, punctate distribution at the cortex (Fig. 8f).

Importantly, the striking defects in cell shape and epidermal tension were not observed in E14.5 *Vangl2* (*looptail*) mutant embryos, suggesting that Wdr1-mediated changes in cortical tension, organization of the actomyosin cortex, and epidermal architecture function upstream of PCP establishment (Fig. 8d,e and Supplementary Fig. 3e).

DISCUSSION

During development, cells and tissues undergo structural, mechanical and geometrical remodelling that can be coupled to cell fate determination, differentiation and proliferation[45,46]. These fascinating mechanisms have been explored predominantly in cultured cells and invertebrate model organisms, and are still poorly understood in mammalian systems *in vivo*. Our study has unearthed pronounced changes in the shape and orientation of epidermal cells that occur within developing mouse skin. Moreover, we showed that the timing of these dynamic changes not only coincides with PCP establishment, but is also physiologically relevant to the process, as reflected by the striking defects in PCP that occur when the shape changes are perturbed.

Our results further unveiled Wdr1 as a major regulator of cell shape dynamics in the skin. Our *in vitro* and *in vivo* data showed that depletion of *Wdr1* increases F-actin content and perturbs the actin cytoskeleton. Interestingly, although loss of *Wdr1* correlates with an increase in endogenous cofilin levels, it ultimately results in a decreased ability to sever F-actin. To understand this seemingly paradoxical result, it is important to note that, although phosphorylation by LIMK diminishes cofilin's activity by abrogating its ability to bind F-actin[47,48], actin severing can be regulated by other means than cofilin phosphorylation[49]. Even when it is bound, cofilin does not necessarily sever F-actin. In fact, dephosphorylated (active) cofilin can form stable F-actin–cofilin structures, as previously reported in several cell types.

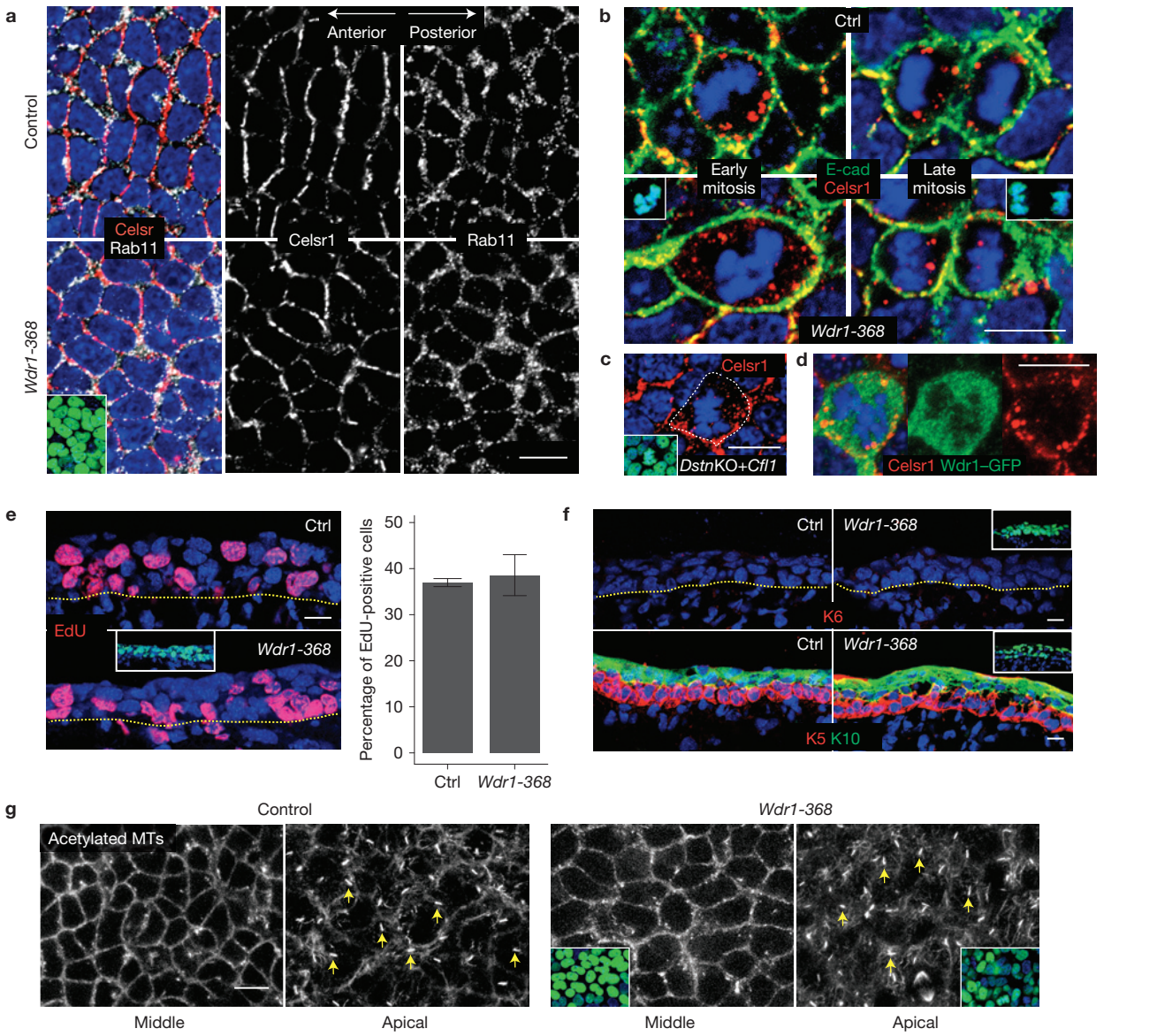

Figure 6 Wdr1 does not affect trafficking of PCP proteins, epidermal differentiation, or proliferation. (**a**) Whole-mount immunofluorescence of E14.5–E15.5 backskins immunolabelled for Celsr1 and Rab11, imaged in the mid-plane of the basal layer. No overt defects in the recycling of Celsr1 to the membrane in *Wdr1*-KD epidermis are observed. (**b**,**c**) Immunofluorescence analysis of mitotic cells reveals no obvious defects in the mitotic internalization of Celsr1 in *Wdr1* KD (**b**), *Dstn*KO+*Cfl1*KD (**c**). (**d**) In Wdr1–GFP-overexpressing epidermis, Wdr1 does not internalize with Celsr1, suggesting that its role in PCP is separate from Celsr1 endocytosis. (**e**) Left, control and *Wdr1-368*-KD embryos, transduced at E9.5, were pulsed for 2 h with EdU at E14.5 and then imaged in 10 μm sagittal sections. Right, quantification of EdU+ cells, revealing no proliferation defects in *Wdr1*-KD epidermis ($P = 0.602$, unpaired *t*-test, $n = 3$ embryos per condition; error bars represent s.d.). (**f**) Immunofluorescence labelling for keratin 6 (K6), a marker induced on hyperproliferation, or co-labelling for basal marker keratin 5 (K5) and differentiation marker keratin 10 (K10) in 10 μm sagittal sections, revealing no defects in differentiation. (**g**) Whole-mount immunofluorescence of backskins labelled for acetylated microtubules (MTs), a marker of primary cilia, and imaged in the mid-plane (left) and apical plane (right) of the basal layer. Results are representative of embryos collected from multiple separate litters. Insets indicate transduced cells (H2B–GFP+ nuclei) except for **b**, where they depict mitoses (DAPI in blue). Dotted lines denote the dermal–epidermal border. Scale bars, 10 μm.

The means by which Wdr1 enhances cofilin-mediated actin severing is a matter of debate. According to one view, Wdr1 and cofilin compete for the same binding site on F-actin, where the role of Wdr1 is to reduce cofilin binding to within an optimal range for severing[10]. Alternatively, Wdr1 could cooperate with cofilin to sever actin filaments rather than compete for the same binding site[24]. Our finding that overexpression of constitutively active cofilin rescues actin severing in Wdr1-deficient cells is compatible with either model, as high levels of active cofilin are likely to override the requirement for Wdr1 either to competitively bind actin or to cooperate with cofilin to promote severing.

The broader polarity and adhesion defects of combined cofilin/destrin deficiency in the skin suggest a special importance of Wdr1 in epidermal cell shape dynamics associated with PCP.

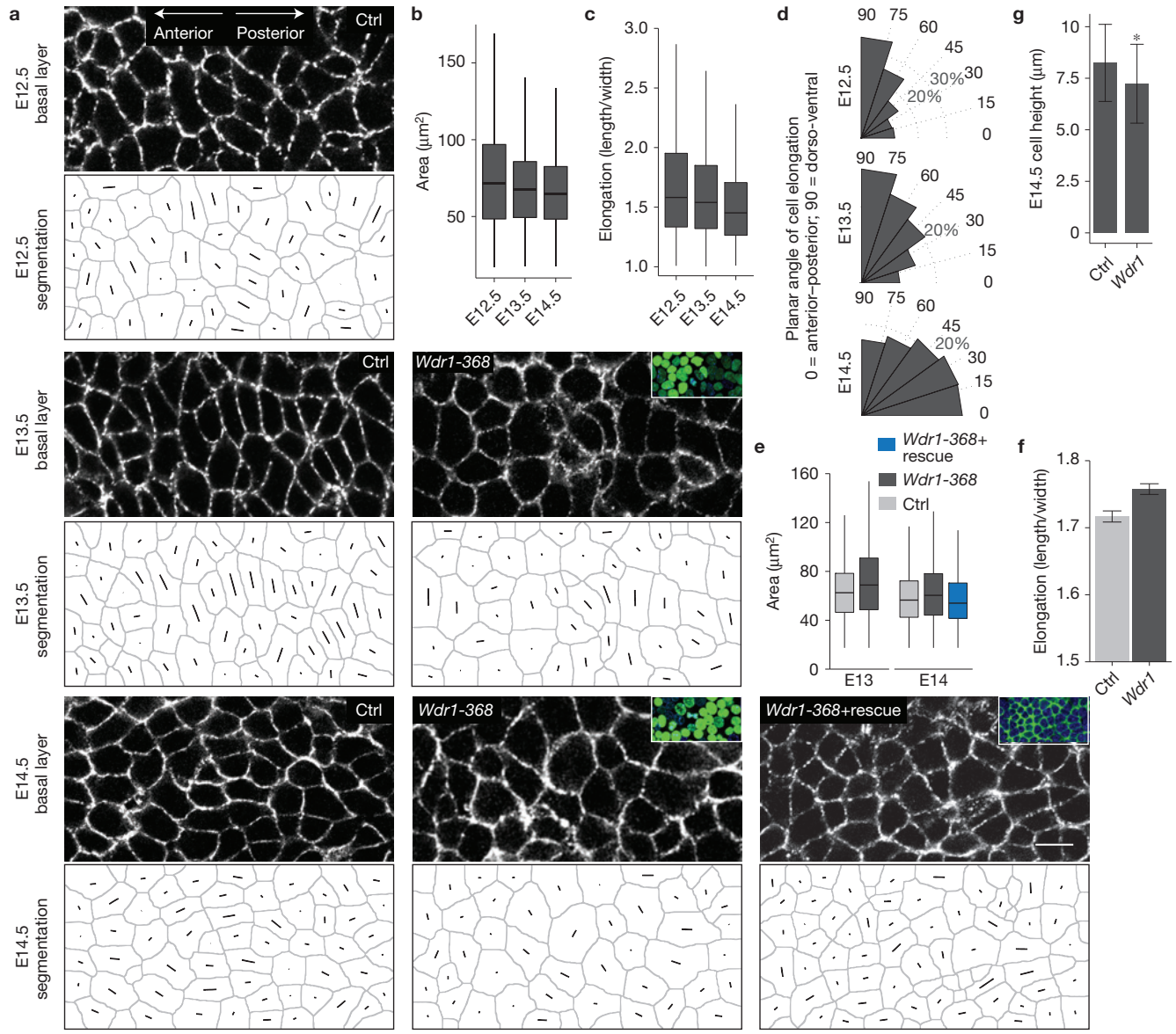

Figure 7 Cell shape dynamics are regulated by Wdr1 and coincide with PCP establishment. (**a**) Representative whole-mount anti-E-cadherin immunofluorescence images of E12.5, 13.5 and 14.5 control backskins, imaged through the centre plane of cells within the basal layer. Each cell's shape and a line through its axis of elongation were computer-generated for quantifications. (**b**–**d**) Quantifications of data from **a**, $n=3{,}238$ cells (E12); $n=2{,}984$ cells (E13); $n=2{,}425$ cells (E14) pooled from at least 4 embryos per condition. (**b**) For cell area, $P=3.9\times10^{-6}$ (E12.5 versus E13.5); $P=6.7\times10^{-6}$ (E12.5 versus E14.5); $P=0.0$ (E13.5 versus E14.5). (**c**) For cell elongation, $p=0.0163$ (E12.5 versus E13.5); $P=0.0$ (E12.5 versus E14.5); $P=0.0$ (E13.5 versus E14.5). (**d**) Histograms of cell orientation relative to the anterior–posterior axis. (**e**,**f**) Analogous experiments and analyses as in **a**–**c** except for Ctrl versus *Wdr1-368* and Ctrl versus *Wdr1-368*+ rescue backskins, $n=3{,}695$ (E13 *scramble*); $n=3{,}085$ (E13 *Wdr1* KD); $n=3{,}683$ (E14 Ctrl); $n=4{,}316$ (E14 *Wdr1* KD); $n=2{,}565$ (*Wdr1*KD+*rescue*) pooled from at least 3 embryos. For cell area in **e**, $P=2.2\times10^{-16}$ (E13.5 Ctrl versus *Wdr1-368*); $P=6.6\times10^{-14}$ (E14.5 Ctrl versus *Wdr1-368*); $P=0.127$ (E14.5 Ctrl versus *Wdr1-368*), ANOVA followed by Tukey's HSD test. (**f**) Cell elongation for E14.5 Ctrl versus *Wdr1-368* basal epidermal cells, $P=0.0008156$ (unpaired *t*-test). (**g**) E14.5 basal progenitor cell heights were calculated from 10 μm sections, $P=0.0007$ for Ctrl versus *Wdr1* KD (unpaired *t*-test). Insets in **a** denote transduced cells (H2B–GFP+). Error bars represent mean ± s.e.m. For box plots in **b**, **c** and **e**, line: median, box: 50% range, whiskers: 1.5× inter-quartile range. Asterisks indicate statistical significance at $P<0.05$. Scale bar, 10 μm.

The architecture of actin networks affects myosin II activity[35], and cofilin competes with myosin II for the F-actin binding site[50]. In line with this, our laser ablation studies demonstrated a significant decrease in boundary tension on loss of Wdr1, suggesting that actomyosin-based tension was reduced. Moreover, as treating embryos with jasplakinolide revealed, increasing F-actin content within the developing embryonic epidermis perturbed rather than enhanced actomyosin tension and probably represented an extreme case of the Wdr1 loss-of-function phenotype. Whether these effects are due to competitive binding of either cofilin or jasplakinolide at the expense of myosin II or more generally to organization of the actin cortex remains to be determined.

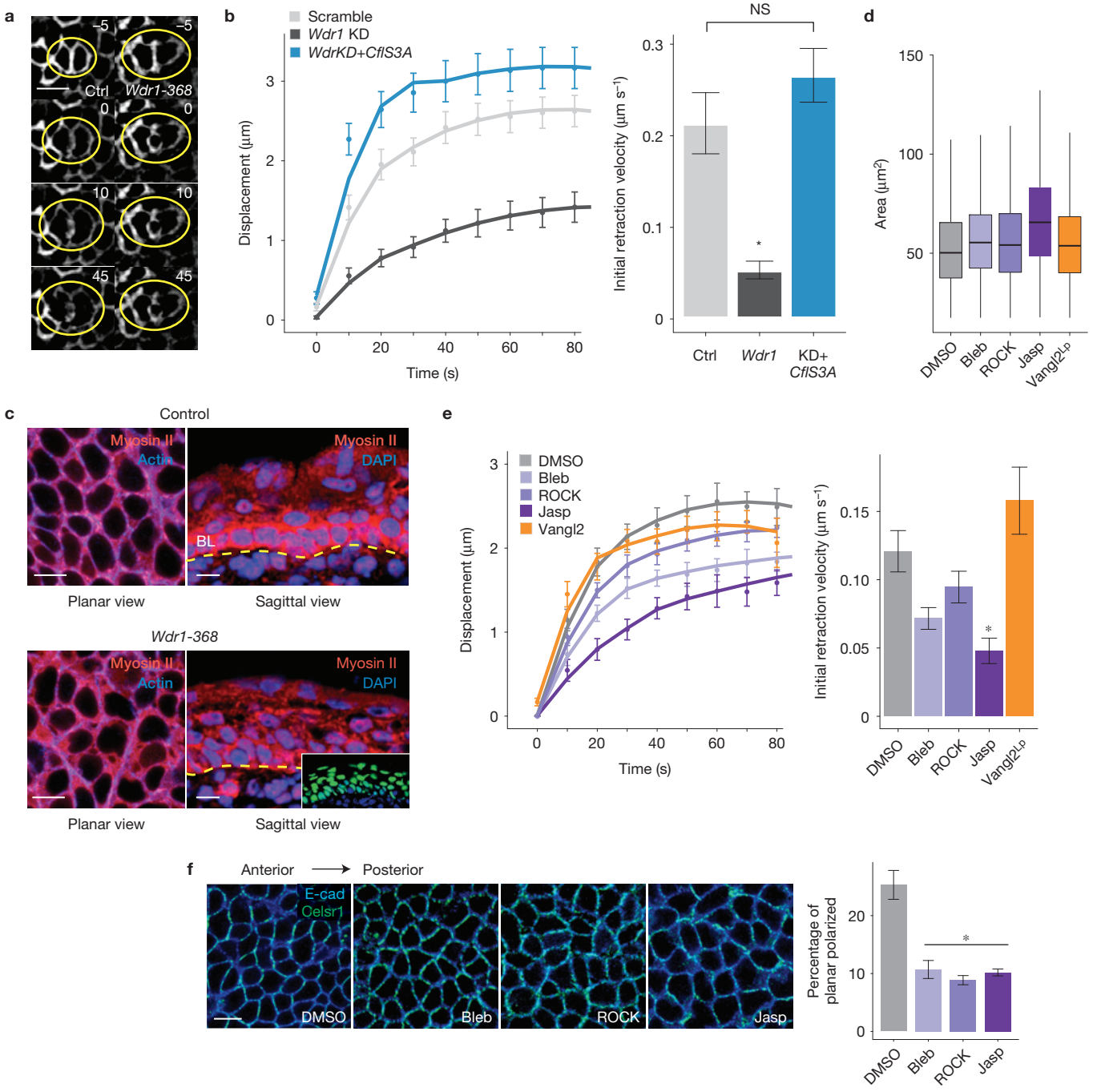

Figure 8 Wdr1 activity is essential for the cell to generate/maintain cortical tension. (**a**,**b**) E9.5 embryos were infected with shRNAs in a membrane-targeted GFP expression vector and subjected to laser ablation at E14.5. (**a**) Representative example of laser ablation in control and *Wdr1-368* epidermis. Numbers represent time in seconds before/after ablation. (**b**) Quantifications of data shown in **a**, $n=15$ (scramble); $n=13$ (*Wdr1* KD); $n=15$ (*Wdr1* KD+CflS3A) ablations per condition. Mean initial retraction velocity: Ctrl, 0.214 μm s^{-1}; *Wdr1-368*, 0.0564 μm s^{-1}, *Wdr1-368+CflS3A*, 0.266 μm s^{-1}. $P=6.1\times10^{-5}$ (Ctrl versus *Wdr1-368*), $P=0.314$ (Ctrl versus *Wdr1-368+CflS3A*), ANOVA followed by Tukey's HSD test. (**c**) Myosin II immunolabelling of E14.5 embryos mosaically expressing *Wdr1-368*. Planar and sagittal views are indicated for untransduced and transduced regions of epidermis. Dotted line, dermo-epidermal border; BL, basal layer. (**d**,**e**) Wild-type mGFP+ embryos at E14.5 were treated with DMSO, jasplakinolide, Y27632 or blebbistatin. All embryos were subjected to cell shape analysis and laser ablation. Data for *Vangl2*-KD embryos are shown for comparison. (**d**) Quantification of cell area, $n=2{,}466$ (DMSO); $n=2{,}764$ (Bleb); $n=3{,}678$ (ROCK); $n=514$ (Jasp); $n=6{,}365$ (*Vangl2^{Lp}*), pooled from at least 3 embryos. (**e**) Mean initial retraction velocities: DMSO, 0.121 μm s^{-1}; Bleb, 0.0716 μm s^{-1}; ROCK, 0.0946 μm s^{-1}; Jasp, 0.0486 μm s^{-1}; and *Vangl2^{Lp}*, 0.158 μm s^{-1}, $P=0.0563$, 0.492, 0.00269 and 0.492, respectively, ANOVA followed by Tukey's HSD test. $n=21$ (DMSO); $n=10$ (Bleb); $n=11$ (ROCK); $n=11$ (Jasp); $n=14$ (Vangl2 KD). (**f**) Celsr1 immunolabelling in whole mounts from E14.5 embryos treated with DMSO, jasplakinolide, Y27632 or blebbistatin. The number of planar-polarized cells is reduced following inhibition of tension in the epidermis. DMSO, 25.3%; Bleb, 10.70%; ROCK, 8.86%; Jasp, 10.20%, $n=4$ embryos per condition. $P=0.00028$, 0.00013 and 0.00022, respectively (ANOVA followed by Tukey's HSD test). Error bars indicate mean ± s.e.m., asterisks indicate statistical significance at $P<0.05$. NS, not significant. Scale bars, 10 μm.

In closing, the link we unearthed between mammalian epidermal cell shape, actin severing, tension and PCP in some ways resembles *Drosophila* wing disc development[6]. However, in contrast to the fly wing disc, intrinsic forces seem to be at the root of this connection in the mouse epidermis. Our additional finding that PCP is linked to Wdr1, cofilins and actin dynamics is interesting in light of the recent surfacing of cofilin (*Cfl1*) in a genetic screen for PCP mutants in the early mouse embryo[30]. However, in contrast to the role for cofilins in orchestrating polarized vesicle trafficking[30], our data indicate that cells within the developing epidermis are under considerable mechanical tension at the time when PCP is established, and rely on a Wdr1/cofilin-based mechanism to govern the actomyosin dynamics that sculpt cell shapes and orient PCP. These findings unveil diversities in the complex relationship between the cells' mechanical and geometrical cues and tissue development. □

METHODS

Methods and any associated references are available in the online version of the paper.

Note: Supplementary Information is available in the online version of the paper

ACKNOWLEDGEMENTS

We thank D. Devenport, S. Williams, S. Beronja, A. R. Folgueras, D. Schramek, I. Matos and E. Ezratty for intellectual input; D. Oristian and A. Aldeguer as mouse specialists; Comparative Bioscience Center (AAALAC accredited) for care of mice in accordance with National Institutes of Health (NIH) guidelines; Bioimaging Center (A. North, director) for advice; Flow Cytometry facility (S. Mazel, director) for FACS sorting. Cfl–GFP was a generous gift from J. Condeelis (Albert Einstein college of Medicine, New York, USA); E.F. is an Investigator of the Howard Hughes Medical Institute. This research was supported by a grant from the NIH (R37-AR27883, E.F.), a Starr Stem Cell Postdoctoral Fellowship (C.L.) and a Genetics Training Grant by the NIH (E.H.).

AUTHOR CONTRIBUTIONS

C.L. and E.F. conceived the study. C.L., E.H. and E.F. designed the experiments. C.L. and E.H. carried out the experiments and analysed the data. H.A.P. performed the ultrastructural analyses (Supplementary Fig. 1S). S.C. made the Wdr1-rescue construct, C.L. and N.S. performed the *in utero* injections. C.L. and M.N. prepared high-titre viruses. C.L., E.H. and E.F. wrote the paper. All authors provided intellectual input, vetted and approved the final manuscript.

COMPETING FINANCIAL INTERESTS

The authors declare no competing financial interests.

Published online at www.nature.com/doifinder/10.1038/ncb3146
Reprints and permissions information is available online at www.nature.com/reprints

1. Eaton, S. & Jülicher, F. Cell flow and tissue polarity patterns. *Curr. Opin. Genet. Dev.* **21,** 747–752 (2011).
2. Goodrich, L. V. & Strutt, D. Principles of planar polarity in animal development. *Development* **138,** 1877–1892 (2011).
3. McNeill, H. Planar cell polarity: keeping hairs straight is not so simple. *Cold Spring Harb. Perspect. Biol.* **2,** a003376 (2010).
4. Devenport, D. & Fuchs, E. Planar polarization in embryonic epidermis orchestrates global asymmetric morphogenesis of hair follicles. *Nat. Cell Biol.* **10,** 1257–1268 (2008).
5. Guo, N., Hawkins, C. & Nathans, J. Frizzled6 controls hair patterning in mice. *Proc. Natl Acad. Sci. USA* **101,** 9277–9281 (2004).
6. Aigouy, B. *et al.* Cell flow reorients the axis of planar polarity in the wing epithelium of Drosophila. *Cell* **142,** 773–786 (2010).
7. Matis, M. & Axelrod, J. D. Regulation of PCP by the Fat signaling pathway. *Genes Dev.* **27,** 2207–2220 (2013).
8. Luxenburg, C., Pasolli, H. A., Williams, S. E. & Fuchs, E. Developmental roles for Srf, cortical cytoskeleton and cell shape in epidermal spindle orientation. *Nat. Cell Biol.* **13,** 203–214 (2011).
9. Fujibuchi, T. *et al.* AIP1/WDR1 supports mitotic cell rounding. *Biochem. Biophys. Res. Commun.* **327,** 268–275 (2005).
10. Chen, Q., Courtemanche, N. & Pollard, T. D. Aip1 promotes actin filament severing by cofilin and regulates the constriction of the cytokinetic contractile ring. *J. Biol. Chem.* **290,** 2289–2300 (2014).
11. Aizawa, H. *et al.* Hyperosmotic stress-induced reorganization of actin bundles in Dictyostelium cells over-expressing cofilin. *Genes Cells* **4,** 311–324 (1999).
12. Augustine, R. C., Pattavina, K. A., Tuzel, E., Vidali, L. & Bezanilla, M. Actin interacting protein1 and actin depolymerizing factor drive rapid actin dynamics in Physcomitrella patens. *Plant Cell* **23,** 3696–3710 (2011).
13. Chu, D. *et al.* AIP1 acts with cofilin to control actin dynamics during epithelial morphogenesis. *Development* **139,** 3561–3571 (2012).
14. Lin, M-C., Galletta, B. J., Sept, D. & Cooper, J. A. Overlapping and distinct functions for cofilin, coronin and Aip1 in actin dynamics *in vivo*. *J. Cell Sci.* **123,** 1329–1342 (2010).
15. Mohri, K. & Ono, S. Actin filament disassembling activity of Caenorhabditis elegans actin-interacting protein 1 (UNC-78) is dependent on filament binding by a specific ADF/cofilin isoform. *J. Cell Sci.* **116,** 4107–4118 (2003).
16. Okada, K., Obinata, T. & Abe, H. XAIP1: a Xenopus homologue of yeast actin interacting protein 1 (AIP1), which induces disassembly of actin filaments cooperatively with ADF/cofilin family proteins. *J. Cell Sci.* **112 (Pt 10),** 1553–1565 (1999).
17. Rodal, A. A., Tetreault, J. W., Lappalainen, P., Drubin, D. G. & Amberg, D. C. Aip1p interacts with cofilin to disassemble actin filaments. *J. Cell Biol.* **145,** 1251–1264 (1999).
18. Kile, B. T. *et al.* Mutations in the cofilin partner Aip1/Wdr1 cause autoinflammatory disease and macrothrombocytopenia. *Blood* **110,** 2371–2380 (2007).
19. Beronja, S., Livshits, G., Williams, S. & Fuchs, E. Rapid functional dissection of genetic networks via tissue-specific transduction and RNAi in mouse embryos. *Nat. Med.* **16,** 821–827 (2010).
20. Curtin, J. A. *et al.* Mutation of celsr1 disrupts planar polarity of inner ear hair cells and causes severe neural tube defects in the mouse. *Curr. Biol.* **13,** 1129–1133 (2003).
21. Kibar, Z. *et al. Ltap*, a mammalian homolog of *Drosophila Strabismus/Van Gogh*, is altered in the mouse neural tube mutant Loop-tail. *Nat. Genet.* **28,** 251–255 (2001).
22. Chen, X. & Macara, I. G. Par-3 mediates the inhibition of LIM kinase 2 to regulate cofilin phosphorylation and tight junction assembly. *J. Cell Biol.* **172,** 671–678 (2006).
23. Michelot, A. *et al.* Actin filament elongation in Arp2/3-derived networks is controlled by three distinct mechanisms. *Dev. Cell* **24,** 182–195 (2013).
24. Nadkarni, A. V. & Brieher, W. M. Aip1 destabilizes cofilin-saturated actin filaments by severing and accelerating monomer dissociation from ends. *Curr. Biol.* **24,** 2749–2757 (2014).
25. Ikeda, S. *et al.* Aberrant actin cytoskeleton leads to accelerated proliferation of corneal epithelial cells in mice deficient for destrin (actin depolymerizing factor). *Hum. Mol. Genet.* **12,** 1029–1037 (2003).
26. Smith, R. S. *et al.* Corn1: a mouse model for corneal surface disease and neovascularization. *Invest. Ophthalmol. Vis. Sci.* **37,** 397–404 (1996).
27. Agnew, B. J., Minamide, L. S. & Bamburg, J. R. Reactivation of phosphorylated actin depolymerizing factor and identification of the regulatory site. *J. Biol. Chem.* **270,** 17582–17587 (1995).
28. Nagaoka, R., Abe, H. & Obinata, T. Site-directed mutagenesis of the phosphorylation site of cofilin: its role in cofilin-actin interaction and cytoplasmic localization. *Cell. Motil. Cytoskeleton* **35,** 200–209 (1996).
29. Kiuchi, T., Ohashi, K., Kurita, S. & Mizuno, K. Cofilin promotes stimulus-induced lamellipodium formation by generating an abundant supply of actin monomers. *J. Cell Biol.* **177,** 465–476 (2007).
30. Mahaffey, J. P., Grego-Bessa, J., Liem, K. F. & Anderson, K. V. Cofilin and Vangl2 cooperate in the initiation of planar cell polarity in the mouse embryo. *Development* **140,** 1262–1271 (2013).
31. Devenport, D., Oristian, D., Heller, E. & Fuchs, E. Mitotic internalization of planar cell polarity proteins preserves tissue polarity. *Nat. Cell Biol.* **13,** 893–902 (2011).
32. Ren, N., Charlton, J. & Adler, P. N. The flare gene, which encodes the AIP1 protein of Drosophila, functions to regulate F-actin disassembly in pupal epidermal cells. *Genetics* **176,** 2223–2234 (2007).
33. Shimada, Y., Yonemura, S., Ohkura, H., Strutt, D. & Uemura, T. Polarized transport of Frizzled along the planar microtubule arrays in Drosophila wing epithelium. *Dev. Cell* **10,** 209–222 (2006).
34. Ross, A. J. *et al.* Disruption of Bardet-Biedl syndrome ciliary proteins perturbs planar cell polarity in vertebrates. *Nat. Genet.* **37,** 1135–1140 (2005).
35. Reymann, A. C. *et al.* Actin network architecture can determine myosin motor activity. *Science* **336,** 1310–1314 (2012).
36. Ono, K. & Ono, S. Two actin-interacting protein 1 isoforms function redundantly in the somatic gonad and are essential for reproduction in Caenorhabditis elegans. *Cytoskeleton (Hoboken)* **71,** 36–45 (2014).
37. Yuan, B. *et al.* A cardiomyocyte-specific Wdr1 knockout demonstrates essential functional roles for actin disassembly during myocardial growth and maintenance in mice. *Am. J. Pathol.* **184,** 1967–1980 (2014).
38. Rhee, J. M. *et al.* In vivo imaging and differential localization of lipid-modified GFP-variant fusions in embryonic stem cells and mice. *Genesis* **44,** 202–218 (2006).
39. Hutson, M. S. *et al.* Forces for morphogenesis investigated with laser microsurgery and quantitative modeling. *Science* **300,** 145–149 (2003).

40. Farhadifar, R., Röper, J-C., Aigouy, B., Eaton, S. & Jülicher, F. The influence of cell mechanics, cell–cell interactions, and proliferation on epithelial packing. *Curr. Biol.* **17,** 2095–2104 (2007).
41. Fernandez-Gonzalez, R., Simoes, S. D. E. M., Röper, J. C., Eaton, S. & Zallen, J. A. Myosin II dynamics are regulated by tension in intercalating cells. *Dev. Cell* **17,** 736–743 (2009).
42. Straight, A. F. *et al.* Dissecting temporal and spatial control of cytokinesis with a myosin II inhibitor. *Science* **299,** 1743–1747 (2003).
43. Ishizaki, T. *et al.* Pharmacological properties of Y-27632, a specific inhibitor of rho-associated kinases. *Mol. Pharmacol.* **57,** 976–983 (2000).
44. Bubb, M. R., Senderowicz, A. M., Sausville, E. A., Duncan, K. L. & Korn, E. D. Jasplakinolide, a cytotoxic natural product, induces actin polymerization and competitively inhibits the binding of phalloidin to F-actin. *J. Biol. Chem.* **269,** 14869–14871 (1994).
45. Heisenberg, C. P. & Bellaïche, Y. Forces in tissue morphogenesis and patterning. *Cell* **153,** 948–962 (2013).
46. Guillot, C. & Lecuit, T. Mechanics of epithelial tissue homeostasis and morphogenesis. *Science* **340,** 1185–1189 (2013).
47. Arber, S. *et al.* Regulation of actin dynamics through phosphorylation of cofilin by LIM-kinase. *Nature* **393,** 805–809 (1998).
48. Yang, N. *et al.* Cofilin phosphorylation by LIM-kinase 1 and its role in Rac-mediated actin reorganization. *Nature* **393,** 809–812 (1998).
49. Moriyama, K. & Yahara, I. The actin-severing activity of cofilin is exerted by the interplay of three distinct sites on cofilin and essential for cell viability. *Biochem. J.* **365,** 147–155 (2002).
50. Wiggan, O., Shaw, A. E., DeLuca, J. G. & Bamburg, J. R. ADF/cofilin regulates actomyosin assembly through competitive inhibition of myosin II binding to F-actin. *Dev. Cell* **22,** 530–543 (2012).

DOI: 10.1038/ncb3146

METHODS

Mouse lines and lentivirus production and injection. The following mouse strains were used: CD1 (Charles River Laboratories) and *Dstn*^{corn1} (Jackson Laboratories). With the exception of *Dstn* KO and *Dstn*KO/*Cfl1*KD embryos, all experiments were performed on E14.5–E18.5 embryos obtained by mating wild-type CD1 males to CD1 females. *Dstn* KO and *Dstn*KO/*Cfl1*KD embryos were obtained by mating homozygous *Dstn*^{corn1} males to homozygous females and injecting with a scrambled-sequence control shRNA or shRNAs against *Cfl1*. Lentiviral shRNAs were obtained from the TRC-1 Library (Sigma). Production and injection of shRNA lentivirus was performed as described previously[19]. Briefly, females at E9.5 of gestation were anaesthetized with isoflurane (Hospira) and the sacs of up to eight embryos per litter were injected with 0.25–1 µl of lentivirus (∼10^9 cfu). The Rockefeller University Animal Care and Use Committee approved animal experimentation protocols used in the study.

Epidermal keratinocytes were isolated and cultured from dispase-treated skins of wild-type CD-1 mice. For *in vitro* infections, cells were plated at 1×10^5 cells per 6-well plate, infected with $>10^9$ cfu lentivirus in the presence of Polybrene. Forty-eight hours after infection, cells were selected with 1 mg ml^{-1} puromycin (Sigma).

The hairpin sequences used were as follows: *Wdr1-368* (TRCN0000108912): 5′-GCTGGGAAGATCAAGGACATT-3′; *Wdr1-1622* (TRCN0000108914): 5′-GATGGCTATTCGGAGAATAAT-3′; Cfl1 (TRCN0000071694): 5′-CGCAAGTCTTCAACACCAGAA-3′; *Vangl2-1738* (TRCN0000124572): 5′-GTTCTGCATTACCCACGACAT-3′.

Immunofluorescence and western blotting. For tissue analyses, skins were frozen and embedded in OCT compound. For immunoreactions, skin sections (10 µM) were blocked with PBS, 0.3% Triton X-100, 1% bovine serum albumin, 5% normal goat serum, 5% normal donkey serum, or MOM Basic kit (Vector Labs). Primary antibodies were incubated for 1 h at room temperature or overnight at 4 °C. Secondary antibodies were incubated at room temperature for 1 h. For whole-mount immunofluorescence microscopy, embryos were fixed for 1 h in 4% formaldehyde, and primary antibodies were incubated overnight at 4 °C.

Immunoblot analyses were performed as previously described[8]. Briefly, proteins were extracted in RIPA buffer. Samples were run on 4–12% gradient gels, transferred to nitrocellulose, and blotted overnight with the indicated antibodies. Blots were scanned on an Odyssey CLx imager (LiCor) and quantified by fluorescence intensity.

Antibodies. Primary antibodies used were: Wdr1 (G-13, Santa Cruz), 1:100; Destrin (ab11072, abcam), 1:100; cofilin (ab42824, abcam), 1:5,000; HPRT (ab10479, abcam), 1:5,000; GAPDH (ab8245, abcam), 1:5,000; GFP (ab13970), 1:2,000; myosin II (PRB-440P, Covance), 1:200; pericentrin (PRB-432C, Covance), 1:1,000; E-cadherin (ECCD-1, M. Takeichi, RIKEN, Japan), 1:500; CD104 (β4 integrin, 553745 BD-Pharmingen), 1:500; P-cadherin (P-cad, Zymed), 1:1,000; Keratin14 (PRB-155P, Covance), 1:1,000; keratin 10 (PRB-159P, Covance), 1:1,000; Celsr1 (Fuchs lab), 1:250; keratin 6 (Rb 415, Millipore), 1:500; PAR3 (07-330, Millipore), 1:100; phospho-S3-Cofilin (77G2, Cell Signaling), 1:5,000; Rab11 (D4F5, Cell Signaling), 1:500; β-actin (AC-15, Sigma), 1:5,000; γ-actin (2-2.1.14.17, Sigma), 1:5,000; α-tubulin (DM1A, Sigma), 1:1,000; acetylated tubulin (6-11B-1, Sigma), 1:1,000. Secondary antibodies conjugated to FITC, rhodamine (Jackson Immunoresearch), or Alexa Fluor 488/546/647 (Invitrogen) were diluted 1:1,000 (sagittal sections) or 1:200 (whole mount), and samples were incubated 1 h–overnight. F-actin was labelled with phalloidin–Alexa Fluor 546/647 (Invitrogen).

Microscopy and image processing. Images were acquired on a Zeiss LSM780 laser-scanning confocal microscope with ×63/1.4 and ×40/1.4 W objectives. Basic image adjustments were performed in Fiji (ImageJ) and Adobe Photoshop CS5. Figures were assembled in Adobe Illustrator CS5.

Quantification of PCP and hair follicle orientation. Whole-mount samples from backskins were processed, labelled for Celsr1 and imaged as described above. Confocal analyses and data collection were conducted at a single horizontal plane through the middle of cells within the basal layer (∼3–4 µm above the basement membrane). Background fluorescence was subtracted and a PCP-polarized cell was defined as a basal layer cell flanked by two distinct and opposing lateral domains of Celsr1. To determine the angle of polarity, the 'straight line' tool in ImageJ was used to draw a line between the centres of the two opposing Celsr1 domains.

To determine the hair follicle orientation, whole-mount samples from backskins were labelled for E-cadherin and imaged at low magnification in *Z*-stacks from the plane of the epidermis to the tips of hair follicles. *Z*-stacks allowed a clear observation of hair follicle angularity. Hair follicles were defined as 'perpendicular' if their angularity was 90° to the basal epidermal plane; for angled hair follicles, the degree of angling was measured by using the ImageJ 'straight line' tool to draw a line between the base of the hair follicle and its tip.

Quantification of F-actin content and actin-severing assays. For measurements of F/G-actin ratios, cells were lysed in F-actin stabilization buffer (50 mM PIPES at pH 6.9, 50 mM NaCl, 5 mM $MgCl_2$, 5 mM EGTA, 5% glycerol, 0.1% NP-40, 0.1% Triton X-100, 0.1% Tween-20, 0.1% beta-mercaptoethanol, 1 mM ATP, protease and phosphatase inhibitor cocktails) at 37°. F-actin was pelleted by ultracentrifugation at 150,000*g*, reconstituted in an equal volume of ice-cold 10 µM cytochalasin D, and incubated on ice for 1 h. Actin in supernatant and pellets was quantified by western blot using G-actin standards (Cytoskeleton).

For actin-severing assays, cells were lysed in buffer containing 50 mM KCl, 2 mM $MgCl_2$, 0.5 mM ATP, 2 mM Tris, pH 8.0, 1 mM EGTA, and 1% Triton X-100 and dialysed (Slide-A-Lyzer 10K, Pierce) to remove detergent. Pyrene-labelled F-actin (Cytoskeleton) was added to cell lysates at a final concentration of 3.8 µM. Pyrene fluorescence was monitored for 1 h using a POLARstar Optima fluorescence plate reader (BMG Labtechnologies) using 355 nm excitation and 405 nm emission filters. Cytochalasin D and jasplakinolide-treated lysates were used as negative and positive controls.

Quantitative analysis of cell area and shape. Measurement of cell area and elongation was performed using custom MATLAB scripts. Confocal images of basal layer epidermis were filtered using a two-dimensional band-pass filter, and cells were segmented on the basis of cortical E-cadherin staining using a watershed algorithm. Cell elongation is defined as the ratio of major and minor axes of automatically segmented cells. For each set of measurements, >2,000 cells were measured from >3 embryos.

Laser ablation. Laser ablation of the cell cortex was performed by targeting an ∼7 µm^2 circular region on a Zeiss LSM 510 NLO system using a Ti:sapphire laser (Chameleon Ultra, Coherent Scientific) tuned to 800 nm. Laser power and dwell time were calibrated per experiment, but were typically performed between 80–100% transmission using scan speed 6 and 50–75 repetitions (∼90–140 µs dwell time).

Pharmacological inhibition of tension. Tension was inhibited in live E14.5 embryos by treating them with 50 µM blebbistatin, 0.5 µM jasplakinolide, 10 µM Y-27632, or an equal volume of DMSO for 6 h in Defined Keratinocyte Medium (Life) with 1.5 mM $CaCl_2$. Embryos were subjected to laser ablation studies or fixed for whole-mount immunostaining.

Electron microscopy. For correlative light and electron microscopy, head skin was carefully dissected out from E16.5 embryos and cut into smaller samples. Samples were fixed in 4% PFA, 0.05% glutaraldehyde in sodium cacodylate buffer for ∼4 h. After washing with PBS, samples were permeabilized and blocked in a solution containing 1% BSA, 0.2% Triton X-100, NH_4Cl 50 mM and incubated overnight in primary antibody (GFP Rabbit IgG Polyclonal Antibody Fraction, Invitrogen, diluted 1:200 in the same solution). Samples were washed and incubated in biotinylated goat anti-rabbit IgG antibody (Vector Laboratories) diluted 1:200 and then processed with the Vectastain ABC reagent (Vector laboratories), using DAB as an enzyme substrate.

For, transmission electron microscopy, samples were fixed in 1% glutaraldehyde in 0.1 M cacodylate buffer, followed by osmium tetroxide fixation and processed for electron microscopy as previously described[8]. Sections (1 µm) were stained for toluidine blue and examined for the presence of cells immunolabelled for GFP. An ultrathin section (70 nm) immediately consecutive to the semithin section was obtained from selected areas from wild-type and WDR1-368 skin respectively. Ultrathin sections were examined at the electron microscope. The area containing exactly the same cells as the semithin section was photographed and analysed at high magnification.

Fluorescence-activated cell sorting. FACS purification of basal epidermal cells from CD1 E14.5 scramble-shRNA; PGK–H2B–GFP-infected mice (Ctrl) or Wdr1-shRNA; PGK–H2B–GFP (KD) was performed on a FACS Vantage SE system equipped with FACS DiVa software (BD Biosciences). Cells were gated for single events and viability and then sorted according to α6 integrin–PE expression and GFP.

For quantification of F-actin levels, primary mouse keratinocytes were infected with *Scramble* or *WDR1*-KD virus, selected with puromycin, trypsinized, fixed and labelled with phalloidin–Alexa Fluor 647.

Semi-quantitative RT-PCR. Equal amounts of RNAs were added to a reverse-transcriptase reaction mix (SuperScript VILO, Invitrogen), and semi-quantitative PCR was conducted with a LightCycler system (Roche Diagnostics). Reactions were performed using the indicated primers and template mixed with the LightCycle DNA master SYBR Green kit and run for 50 cycles. Specificity of the reactions was determined by subsequent melting curve analysis. LightCycle analysis software was used to remove background fluorescence (noise band). The number of cycles needed to reach the crossing point for each sample was used to calculate the amount of

each product using the 2–CP method. Levels of PCR product were expressed as a function of Ppib and/or HPRT expression. Sequences of primers used were as follows: *Wdr1*, forward: 5′-TGGAGCGGGGCGTCTCTA-3′, reverse: 5′-AATCCGCTGGGTGCATACTTG-3′; *Cfl1*, forward: 5′-ATGCACCCCTCAAGAGCAAAAT-3′, reverse: 5′-AGGGGGTGGGAGGGATGTT-3′; *Actb*, forward: 5′-CGGCCAGGTCATCACTATTGG-3′, reverse: 5′-AGGGGCCGGACTCATCGTA-3′; *Actg1*, forward: 5′-CCCAAAGCTAACAGAGAGAAGATGACG-3′, reverse: 5′-GTGGTAAAGCTGTAGCCCCGTTCA-3′; *Myh9*, forward: 5′-CCTGCCATAAGGGAACCTAATCAC-3′, reverse: 5′-GCGCTCTGGTGCCTCTCCTA-3′; *Krt14*, forward: 5′-CGCCGCCCCTGGTGTGG-3′, reverse: 5′-ATCTGGCGGTTGGTGGAGGTCA-3′; *Cdh1*, forward: 5′-GATGATGCCCCCAACACTCC-3′, reverse: 5′-CTCTCGAGCGGTATAAGATGTGATTT-3′; *Pard6g*, forward: 5′-CAAGCCTGGGAAGTTTGAAGATTT-3′, reverse: 5′-TGCGGCATGCTGATGTTGA-3′; *Prkcc*, forward: 5′-CAGCGACAGAGAAAACTTCCTGAA-3′, reverse: 5′-TCCCGCCATCATCTCAAACATA-3′; *Gpsm2*, forward: 5′-TCTGCTGCAAAGAGATCCAAACA-3′, reverse: 5′-TCATGGGCAGGTACAAAAAGTCC-3′; *Celsr1*, forward: 5′-GGCAGTCATGACCTTGGACTA-3′, reverse: 5′-AGCTGATTCCCAATCTGCAC-3′; *Vangl2*, forward: 5′-CCAGCCGCTTCTACAATGTC-3′, reverse: 5′-TCTCCAGGATCCACACTGC-3′; *Dvl2*, forward: 5′-ACTTCACCCTCCCTCGAAA-3′, reverse: 5′-GAGGAGCCAGGGTAAGCAG-3′; *Fzd6*, forward: 5′-TTAAGCGAAACCGCAAGC-3′, reverse: 5′-TTGGAAATGACCTTCAGCCTA-3′; *Ki67*, forward: 5′-CCCAGCTCGTCTCCACCACTAGAG-3′, reverse: 5′-TCTGTGTGTTTCTGGTTTGCCTTAC-3′; *HPRT*, forward: 5′-GATCAGTCAACGGGGGACATAAA-3′, reverse: 5′-CTTGCGCTCATCTTAGGCTTTGT-3′; *Ppib*, forward: 5′-GTGAGCGCTTCCCAGATGAGA-3′, reverse: 5′-TGCCGGAGTCGACAATGATG-3′.

Quantification of cell proliferation. E14.5 *Scr*- or *Wdr1*-shRNA-infected embryos were pulsed with 5 µl g^{-1} 5-ethynyl-2′-deoxyuridine (EdU) (Click-iT EdU Cell Proliferation Assays, Life Technologies) for 2 h. Samples were frozen in OCT, sectioned (10 µm) and processed according to the manufacturer's instructions. The ratio between EdU+/GFP+ (for *WDR1*- or *Scr*-infected) cells and nuclei number (DAPI+) was calculated.

Statistics. Quantitative data were statistically analysed (mean and s.e.m.) and compared using a paired or *n* unpaired *t*-test (two experimental groups), or ANOVA followed by Tukey's honest significant difference test (multiple groups) in Microsoft Excel or the R statistical environment. Sample sizes and the specific tests performed are indicated in the figure legends. No statistical method was used to predetermine sample size, experiments were not randomized, and investigators were not blinded to allocation during experiments and outcome assessments.

DOI: 10.1038/ncb3146

nature cell biology

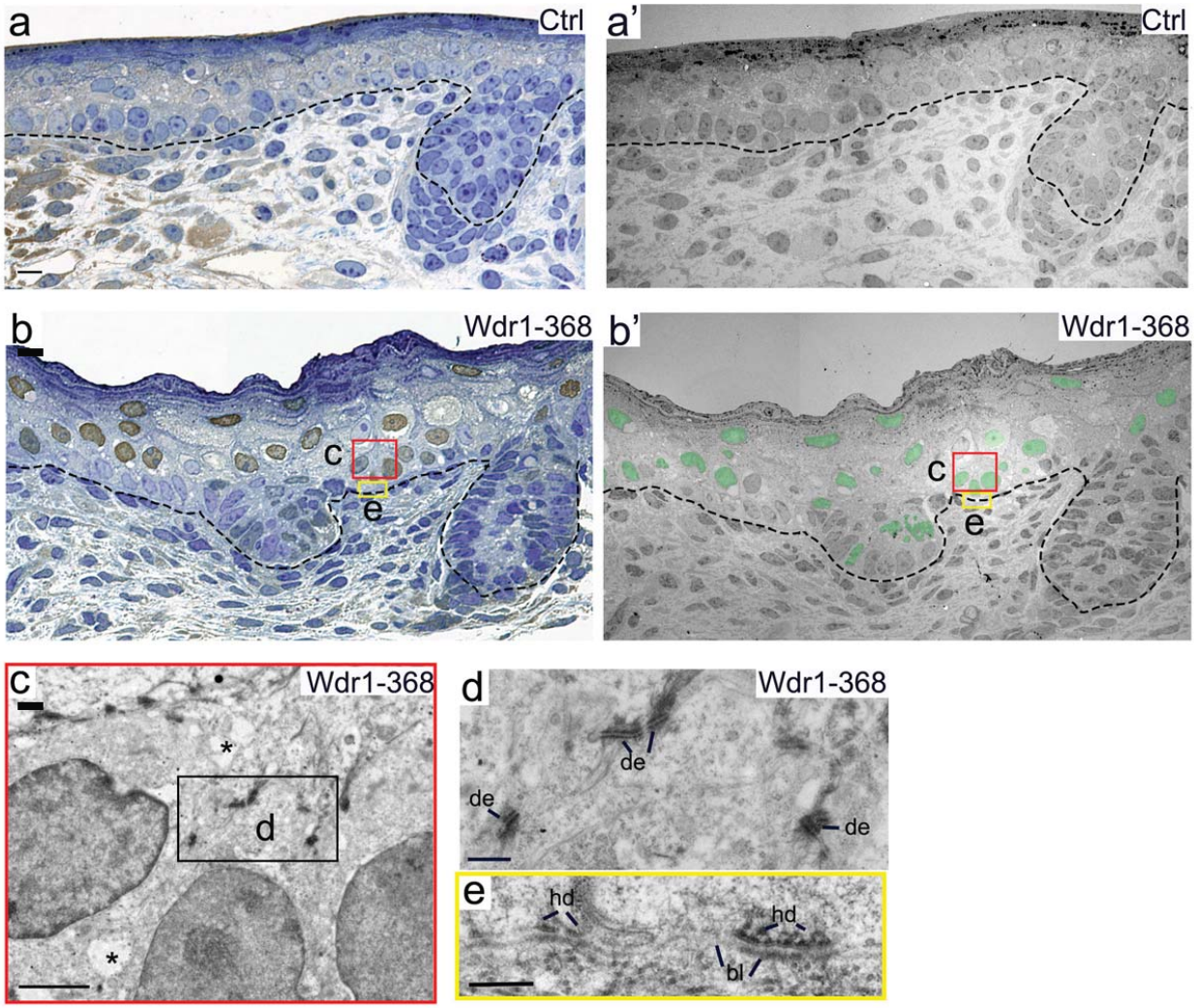

Supplementary Figure 1 *Wdr1* knockdown epidermis display normal intercellular adhesion and attachment to the basement membrane. Correlative light and electron microscopy of E16.5 headskin in WT and *Wdr1-368*. Whole mount skin was immunolabeled for GFP (and subsequently embedded for electron microscopy. (a) and (b) Semithin sections (1 µm) were stained with toluidine blue and examined for the presence of GFP positive cells (brown nuclei). Dotted line indicated dermo-epidermal boundary. (b and b') consecutive ultrathin sections were examined at the electron microscope. For *Wdr1-368*, the same exact cells that were GFP+ by immunohistochemistry were identified (pseudocolored in green) and photographed at high resolution. Red box enlarged in (c) and yellow box enlarged in (e). (c) Epidermal cells in *Wdr1-368* display normal adhesion, with intact desmosomes (de) shown in boxed area enlarged in (d) No gaps were observed between the cells. Some inevitable cytoplasmic damage (asterisks) is due to detergent permeabilization necessary for immunolabelling. (e) Electron microscopic analysis showed intact basal lamina (bl) and hemidesmosomes (hd). Bars in (a) and (c), 2 µm, also valid for a', b and b'. Bars in (d) and (e), 500 nm.

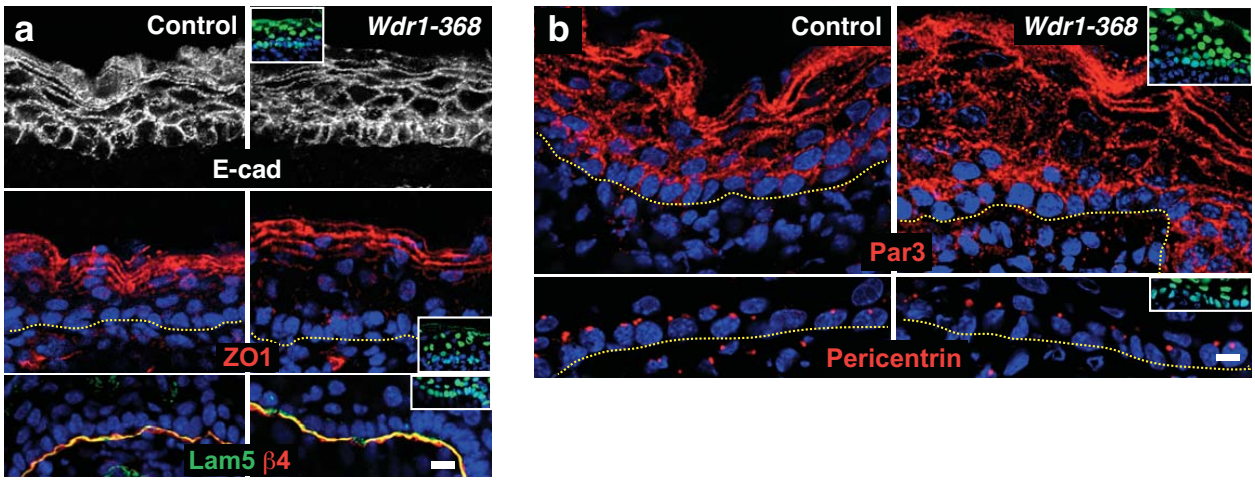

Supplementary Figure 2 Normal adhesion and apicobasal polarity in *Wdr1* knockdown epidermis. 10μm sagittal sections of E16.5 backskins were labelled for: (a) E-cadherin (E-cad) or ZO1 and co-labelled for integrin β4 (β4) and Laminin 5 (Lam5) (b) ABP markers Par3 and pericentrin. DAPI was used to label chromatin. Dotted line denotes the dermal-epidermal border. Inserts denote infected cells (H2B-GFP+ nuclei). Scale bar, 10μm.

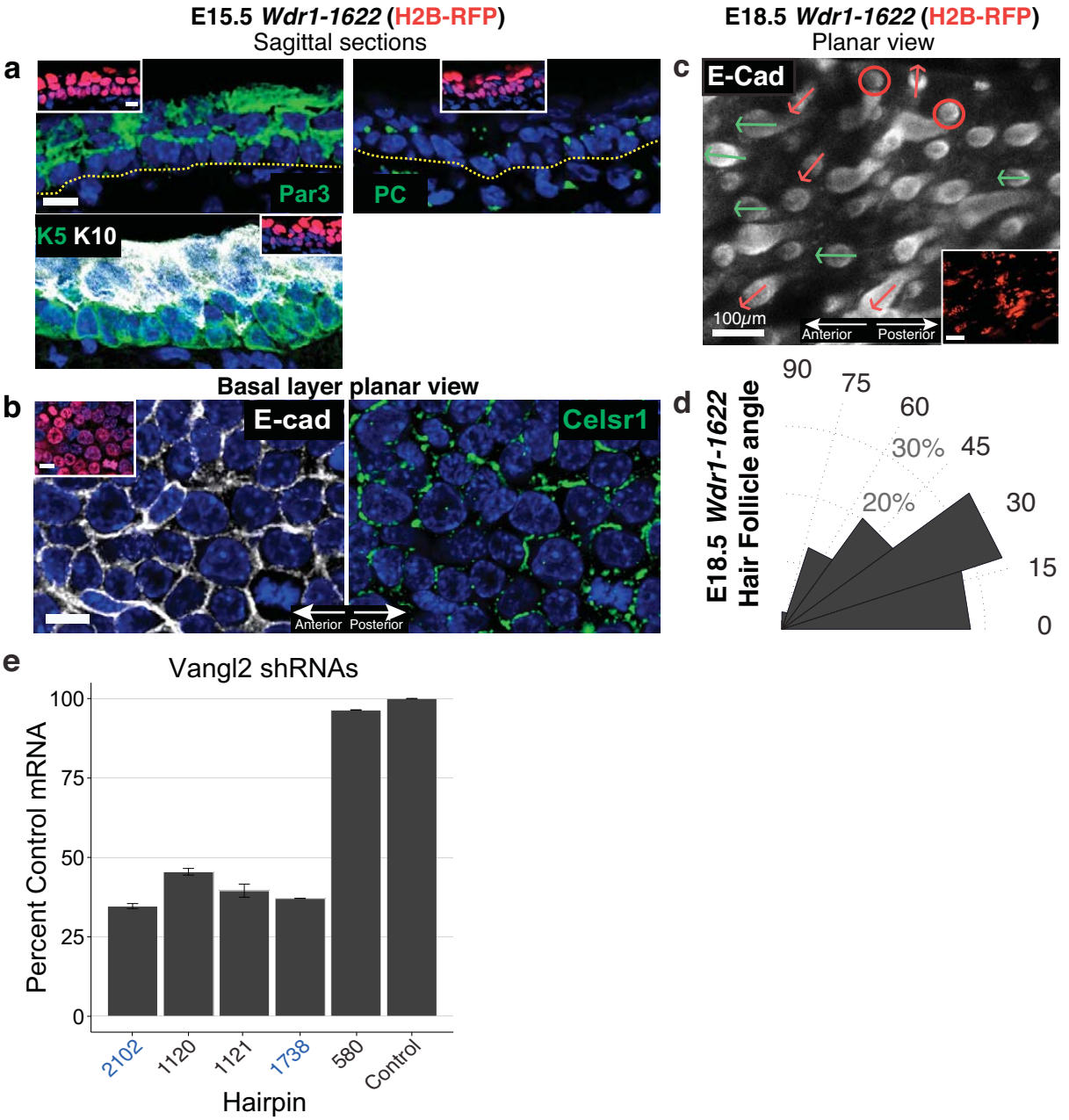

Supplementary Figure 3 *Wdr1* knockdown by a second hairpin (*Wdr1*-1622) results in PCP defects analogous to *Wdr1*-368 and validation of *Vangl2* shRNAs. (a) 10 μm sagittal sections of E15.5 backskins were labelled for Par3 or Pericentrin (PC) or co-labelled for Keratin 5 (K5) and Keratin 10 (K10). (b) Whole-mount immunofluorescence of E15.5 backskins co-labelled for E-cadherin (E-cad) and Celsr1 and imaged in the mid-plane of the basal layer. (c) Whole-mount immunofluorescence of E18.5 HFs labelled for E-cadherin. (d) Quantifications of data shown in (c), *n*=36 hair follicles from 3 embryos. Note similarities to data compiled on similarly aged *Wdr1-368* knockdown embryonic epidermis (see Figures 1 and 2). Green arrows denote normal HF orientation, red arrows denote abnormal HF orientation. Red circles denote perpendicularly oriented HFs. Insets denote transduced cells (H2B-RFP+ nuclei). (e) *In vitro* Knockdown efficiencies of shRNAs against Vangl2 to achieve specific loss of PCP in the skin, *n*=3 independent measurements/hairpin. Error bars indicate mean ± s.e.m. Scale bars, 10μm.

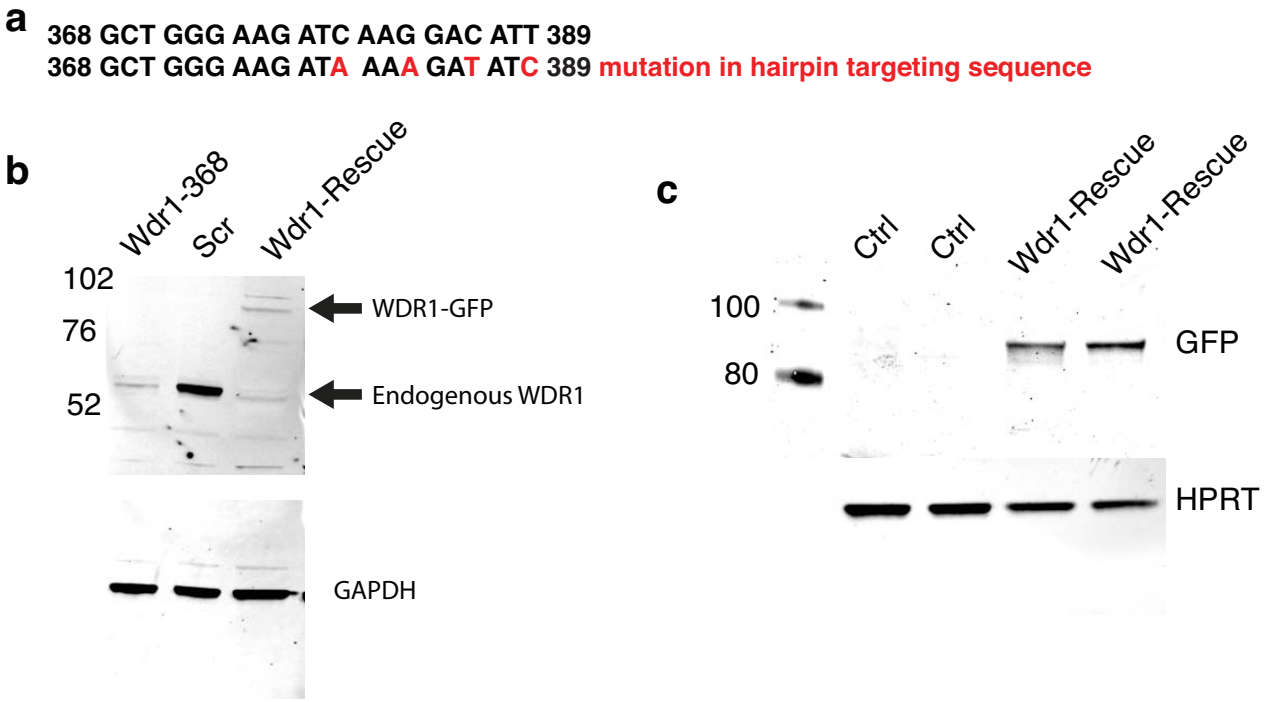

Supplementary Figure 4 Generation and expression of a hairpin-resistant *Wdr1-GFP* lentiviral transgene. (a) *Wdr1* coding sequence recognized by *Wdr1-368* hairpin and a mutant, shown in red, that renders it refactory to the hairpin. (b, c) Western blots of protein extracts from WT cells or cells transduced with lentiviruses that contain either *Wdr1-368* shRNA, *Scrambled* control shRNA or the *Wdr1-GFP* hairpin-resistant mutant cDNA expression vector. Blots were probed with WDR1 antibodies (Ab) (b) or GFP Ab (c). Note the ~93kDa WDR1-GFP protein (endogenous WDR1=66kDa, GFP=27kDa) detected with both Abs. Glyceraldehyde dehydrogenase (GAPDH) and hypoxanthine-guanine phosphoribosyltransferase (HPRT) Abs were used as loading controls.

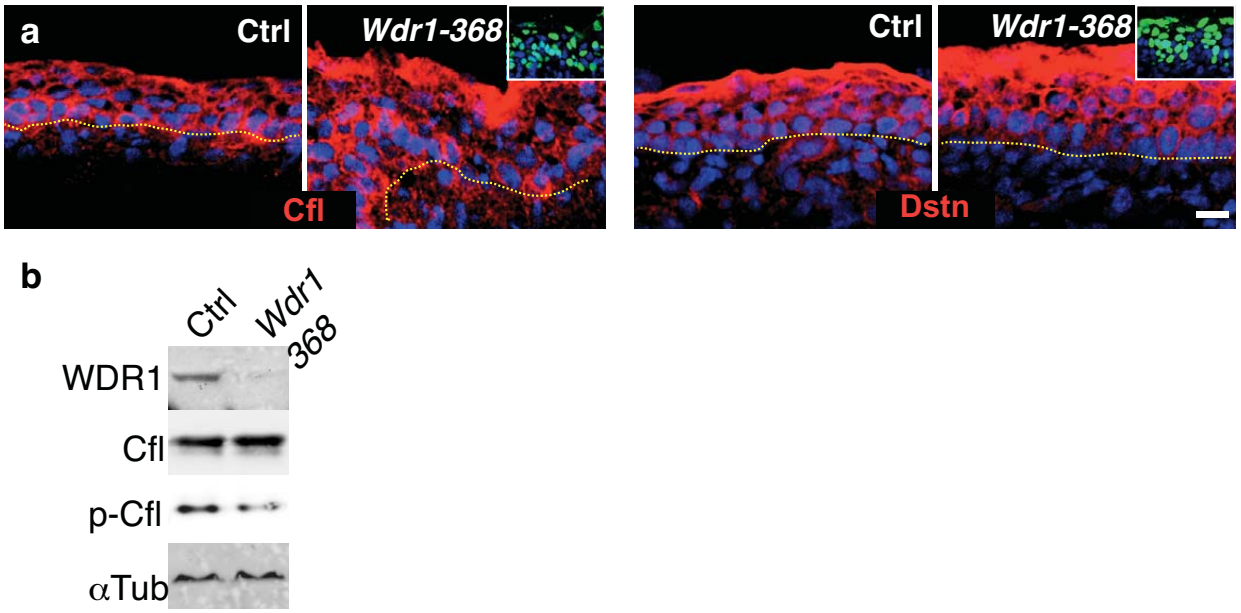

Supplementary Figure 5 Normal localization of Cofilin and Destrin in *Wdr1-368* KD epidermis. (a) 10 µm sagittal sections of E15.5 control and *WDR1-368* KD backskins were labelled for Cofilin (Cfl) or Destrin (Dstn). Inserts denote transduced cells (H2B-GFP+ nuclei). DAPI in blue. (c) Western blot analyses of protein extracts from control (*Scr*) and *Wdr1-368* KD 1^0MK were probed with antibodies against: WDR1, Cofilin (Cfl) phospho-serine 3-cofilin (p-Cfl) and α-tubulin (αTub, loading control). (d) qPCR of mRNAs were from control and *Cfl1*KD/*Dstn*-null (KD/KO) 1^0MK. n=3 samples/condition *Cfl1* levels in Ctrl vs. KD/KO p=0.0026; *Dstn* levels in Ctrl. vs. KD/KO p=0.009. Dotted line denotes the dermal-epidermal border. Insets show transduced cells (H2B-GFP+ nuclei). Scale bars, 10µm.

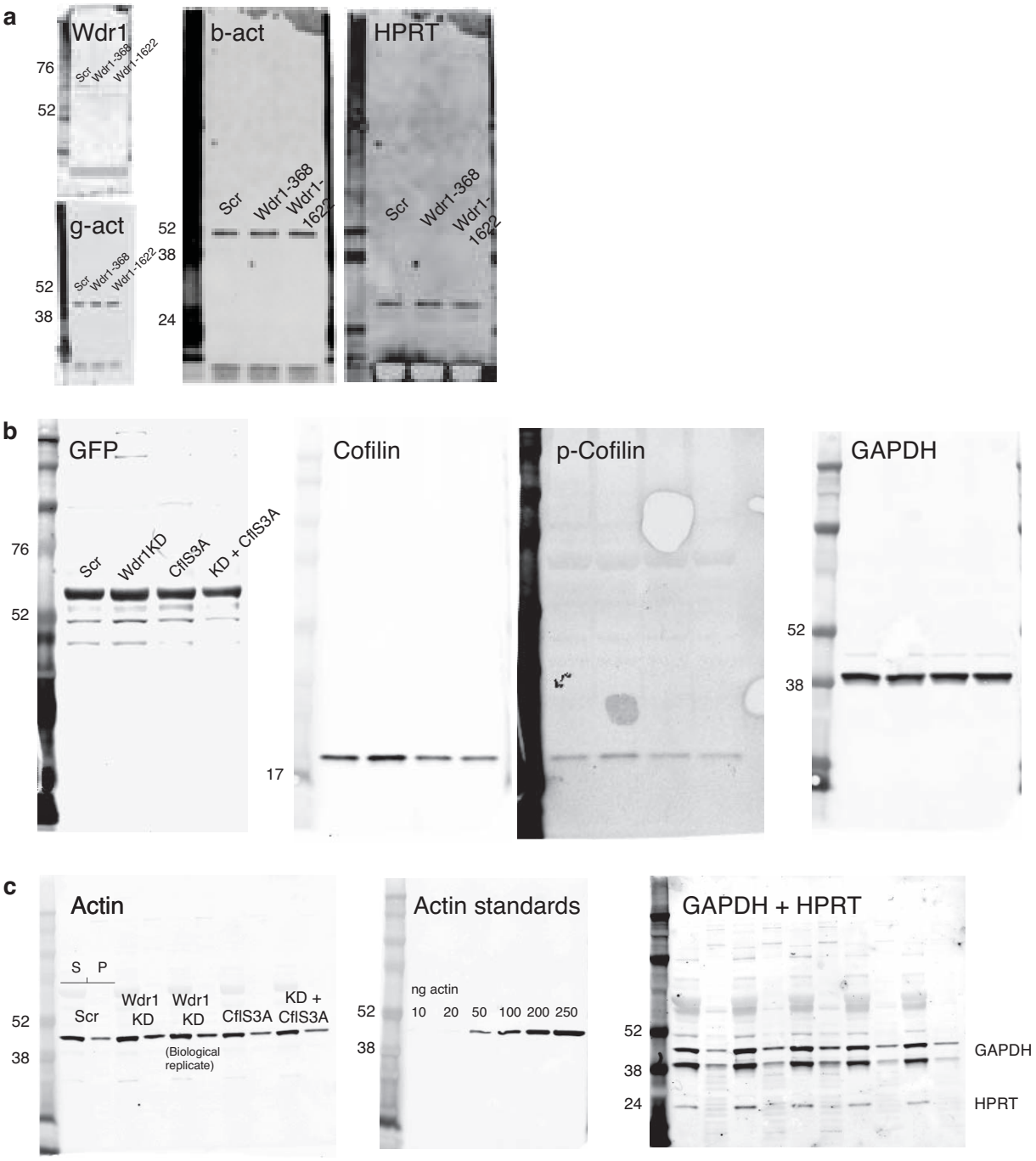

Supplementary Figure 6 Quantification of F-actin content, actin severing, and endogeneous levels of cofilin in *Wdr1-KD* and cofilin-overexpressing keratinocytes. (a) Uncropped Western blots used to evaluate Wdr1 knockdown and endogeneous levels of actin in Figure 1A. (b) Uncropped Western blots used to evalulate endogeneous cofilin and phosph-cofilin levels in transduced keratinocytes in Figure 5a-b. Immunoblot for GFP indicates overexpression of histone 2B (H2B)-GFP (~51 kDa), used as a marker of lentiviral transduction in scramble- and *Wdr1*-KD keratinocytes, and overexpression of *GFP-CflS3A* (~52 kDa) in the others. Relative levels were quantified by fluorescence intensity on a LiCor Odyssey CLx imager and normalized to GAPDH levels. (c) Uncropped Western blots used to quantify F/G actin ratios. G-actin standards were loaded at the indicated quantities and used to construct a calibration curve. Actin levels were normalized to the cytoplasmic HPRT signal in each lysate.

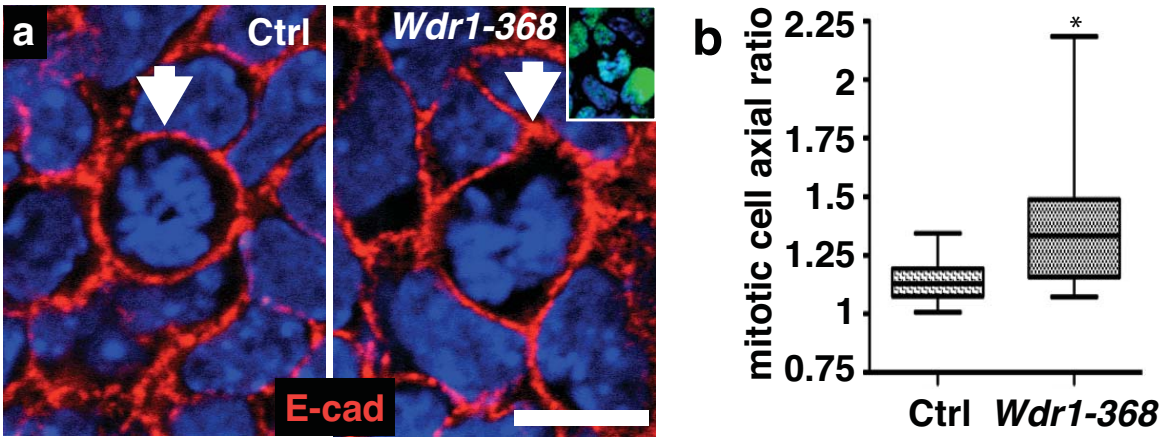

Supplementary Figure 7 Defects in mitotic rounding in *Wdr1-368* KD epidermis. (a) Whole-mount immunofluorescence of E15.5 backskin labeled for Ecadherin (E-cad) and imaged at the basal layer plane. (b) Quantifications of data from (a). Control: 1.14±0.088; *Wdr1 KD*: 1.39±0.27, p=5.27X10^{-5} (unpaired t-test), *n*=23 cells (WT); *n*=29 cells (Wdr1 KD) from 3 embryos per condition. Box and whiskers plot: line=median, box=50% range, whiskers=100% range. Arrow denotes early mitotic cells. Inserts denote infected cells (H2B-GFP+ nuclei). Scale bar, 10μm.

Supplemental Table 1: Phenotypic analysis of the *Wdr1/Destn/Cfl1* pathway

Genetic Manipulation	Cell-Cell Adhesion	Multinucleated cells	ApicoBasal Polarity	% of E15.5 PCP (Celsr1 distribution)
Control	+	-	+	63
Wdr1 (KD)	+	-	+	34
Cfl1 (KD)	+	-	+	55
Dstn^{tm1}KO	+	-	+	52
Cfl1 (KD) + *Dstn*^{tm1}(KO)	-	+	-	5.4
Wdr1 (KD)+*Dstn*^{tm1}(KO)	-	+	-	5.2
Cfl1-S3A-GFP (OE)	+	-	+/-	40
Wdr1 (KD) +*Cfl1-S3A-GFP* (OE)	+	+	+	48

KD= knockdown
KO= knockout
OE= overexpression

Supplemental Table 1 Phenotypic analysis of the *Wdr1/Destn/Cfl1* pathway.
Summary of the epidermal phenotypes of the *Wdr1/Destn/Cfl*1 pathway. While the combined loss of cofilin family-members leads to disruptions in apicobasal polarity and adhesion, loss of *Wdr1* only affects planar polarity.